AD-A099 167 SCIENCE APPLICATIONS INC LA JOLLA CA F/G 20/6
FURTHER STUDIES ON NONLINEAR ADAPTIVE OPTICS,(U)
APR 81 A ELCI, J NAGEL, D ROGOVIN F49620-79-C-0027
UNCLASSIFIED AFOSR-TR-81-0464 NL

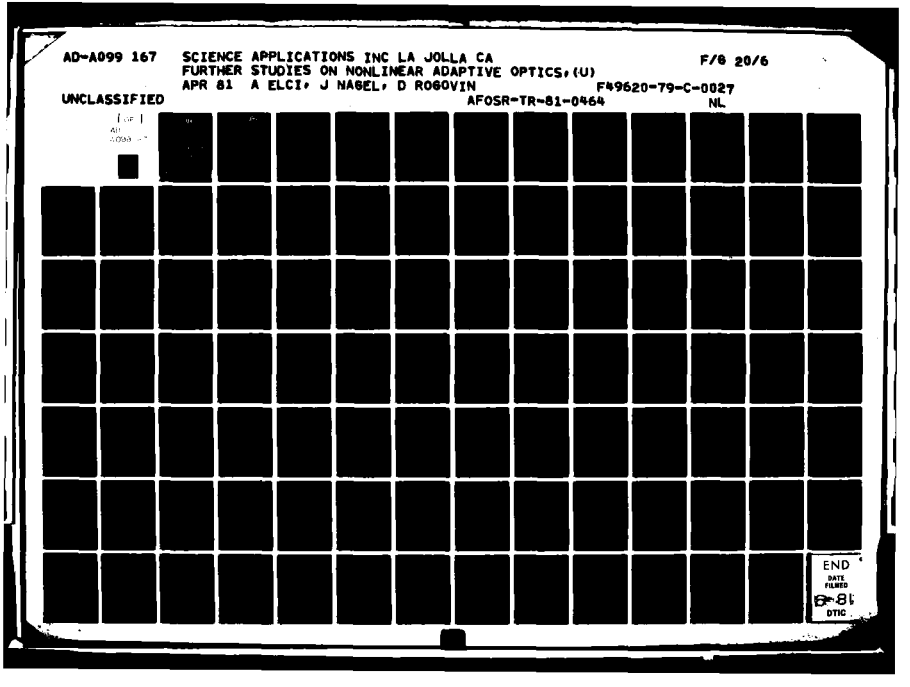

END
DATE FILMED
6-81
DTIC

LEVEL II

12

4

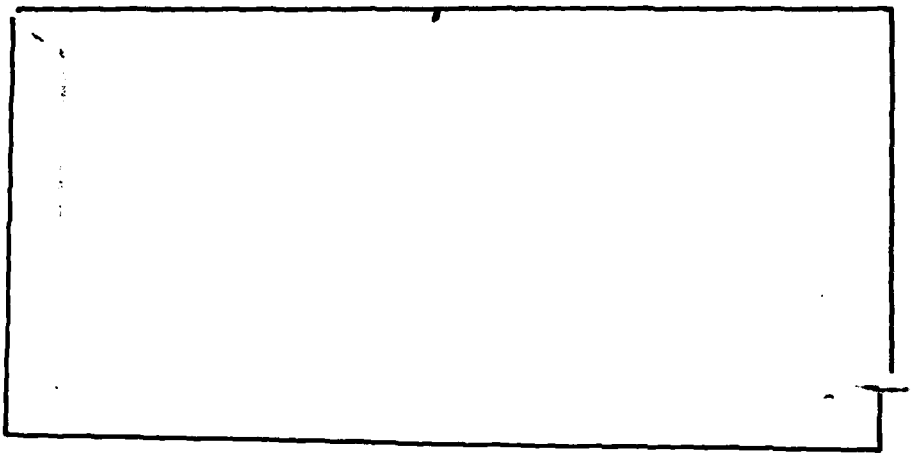

SCIENCE APPLICATIONS, INC.

LEVEL II

(12)

(18) AFOSR (19) TR-81-0464

(6) FURTHER STUDIES ON

NONLINEAR ADAPTIVE OPTICS

(11) April 1981

(15) F49620-79-C-0027

Submitted to:

Director of Physics
Air Force Office of Scientific Research
ATTN: NP
Bldg. 410, Bolling AFB
Washington, D.C. 20332

Submitted by:

(10) A. Elci, J. Nagel, D. Rogovin
Science Applications, Inc.
1200 Prospect Street
La Jolla, California 92038

(12) 95

TABLE OF CONTENTS

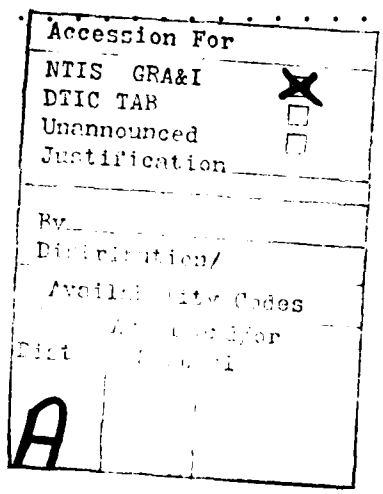

FURTHER STUDIES ON
NONLINEAR ADAPTIVE OPTICS

by:

A. Elci, J. Nagel and D. Rogovin

Science Applications, Inc.
1200 Prospect Street
La Jolla, California 92038

Abstract: This work examines interband transitions near the bandedge, alkali type ious embedded in dielectrics, and two-photon resonances in three-level systems for the purpose of four-wave mixing and phase conjugation at the iodine laser frequency. It also examines the time-dependent properties of unstable resonators with a saturable gain medium. The third order susceptibility and the conjugate reflectivity of semiconductors are calculated. Near the band edge the reflectivity is enhanced. The unstable-resonator field is represented in terms of a series of empty resonator modes, and a set of first order in time differential equations for the exapansion coefficients is achieved. There is a stable solution and a bistable one, with self-sustaining pulsations.

I. STATEMENT OF WORK

a. Examine non-linear materials, particularly liquids and gasses for candidates for high efficiency, degenerate, four-wave mixing media for use with an Iodine (I*) laser. Several such candidates are:

1. Nd-YAG

2. I*

3. Two-photon resonant dyes

4. Two-Photon resonant metal vapor

5. Excited state alkalai metal

b. Consider the above materials and such others that may arise in the study, or be suggested by the Air Force Weapons Laboratory.

c. Consider systems that might emulate a potential non-linear medium at a frequency that is experimentally attainable, i.e., a D.F. frequency.

d. Modeling of the media selected will be developed in conjunction with experiments at the Air Force Weapons Laboratory.

e. Analyze the effects of transverse mode competition in unstable resonator lasers using Lamb Theory of the Active medium and actual unstable resonator mode functions.

II. NONLINEAR ADAPTIVE OPTICS SUMMARY

The results of our work on nonlinear adaptive optics are given in two papers: "Novel Approaches to Nonlinear Adaptive Optics at 1.3μ", which will be published in the Proceedings of the International Conference on Lasers '80, New Orleans, and in "Four-Wave Mixing Near the Band Edge", which is submitted for publication. These papers are reproduced in this report as Appendices 1 and 2.

We examined two-photon resonances for the purpose of four-wave mixing and found that the third-order susceptibility is typically two orders of magnitude less than what is practically desired. We therefore searched for alternative means, particularly for phase conjugation at the iodine laser wavelength, 1.3μ.

An alternative method uses the interband transitions near the band edge. We found that the reflectivity for conjugate waves is resonantly enhanced near the band edge. If the frequency of the light is near the band edge, large, third-order susceptibilities and reflectivities are obtained. To match 1.3μ, a particularaly promising material turns out to be $(Ga_x\ In_{1-x})As$, which is a semiconductor compound with a direct band gap at the center of the Brilloin zone. The size of the gap can be varied by changing the alloy composition. It is therefore possible to match the band gap and the iodine laser frequency as closely as desired. The reflectivity, as it turns out, has a simple Lorentz factor near the band edge, which leads to the resonant enhancement. When $x \sim 0.6$, the $(Ga_xIn_{1-x})As$ band gap approximately matches 1.3μ. The third order susceptibility is then about 10^{-6} esu, which is a substantial amount.

The calculations we have performed are sufficiently general so that they can be adapted to other semiconductors.

We also considered another method to match 1.3μ with a single photon resonance of a nonlinear medium. Foreign atoms embedded in solids or liquids strongly interact with their surroundings and therefore, the relative spacing of their atomic levels can be drastically altered. By choosing the proper solid or

liquid, and a foreign atom, it is possible to match 1.3μ with an atomic transition. For this purpose we have considered alkali ions embedded in solid dielectrics. A promising system like this has an additional advantage. Most of the absorption at 1.3μ is due to the Na^I themselves. By controlling the number of Na^I in the sample, it is possible to have a system which can easily be saturated at 1.3μ.

III. TRANSVERSE MODE COMPETITION IN GAIN DRIVEN UNSTABLE RESONATORS

The analysis, calculations, results and discussion are presented in Appendix 3, which is a preprint of a paper submitted to the Journal of the Optical Society of America. Below we summarize the results of the project.

The calculation hinges on the expansion of the field in an unstable resonator with a saturable gain medium in terms of a series of empty resonator modes. Substitution into the Maxwell equations yields, after some reductions, a set of first order differential equations for the time dependence of the expansion coefficients. The diffraction losses are included in a natural way and the results are physically transparent.

The equations are coupled together by overlap integrals involving the empty resonator modes and the nonlinear, field dependent susceptibility. The integrals range over longitudinal and transverse coordinates, and hence are quite complicated. However, if the empty resonator modes are assumed to be known in advance and can be stored on disc, the calculation is much easier than the numerical evaluation of the nonlinear Fresnel-Kirchoff transform. The necessary accuracy for the evaluation was determined, and it was found that the grid size requirements for the longitudinal integration were two orders of magnitude less stringent than for the transverse integration.

Calculations were carried out for M = 2 cavities with $N_{eq} = 6.5$ and $N_{eq} = 7.02$. These two values of equivalent Fresnel number were chosen because they are the locations of a peak and a crossing point of the eigenvalue versus equivalent Fresnel number plot. The lowest loss empty resonator modes for the $N_{eq} = 6.5$ cavity is well separated from the others, and thus we expected that this mode would dominate the laser operation. In the calculations this indeed occurred, with about 95% of the energy concentrated in the lowest loss modes. The higher order modes were found to affect strongly the output coupling, frequency pulling, and linewidth of the laser, but not the distribution of energy.

By contrast, for the $N_{eq} = 7.02$ cavity the two lowest loss modes have equal losses, and the posibility of unstable behavior was considered. Bistable operation was found to occur in a small region of pumping strengths, with stable solutions on either side of this region. In the region of small gain both modes were found to be oscillatory, and above the bistable regime one of the lowest loss modes was suppressed. In the region of bistability itself, self-sustaining pulsations were found to occur for most initial conditions of the laser system. The iterative solution of the equations of motion did not converge to a stable point in these cases, but to a well defined limit cycle. This type of behavior is well known in laser systems and is a result of nonlinearity. This is the first demonstration of nonlinear oscillations arising from competition between transverse modes.

The formulation of the equations of motion of unstable laser resonators in Lamb Theory form has been shown to be useful both qualitatively and quantitatively. Physically, the idea of expressing the laser energy distribution as a superposition of empty resonator modes is appealing. Bistable behavior and self-sustaining pulsations result naturally from this model. The numerical results are expected to be most accurate when one of the modes manages to suppress all the others. Quantities such as frequency pulling, laser linewidth, and output coupling are given, as well as the stable distribution of radiation in the cavity.

APPENDIX 1

NOVEL APPROACHES TO NONLINEAR ADAPTIVE OPTICS AT 1.3μ

by

A. Elci and D. Rogovin

NOVEL APPROACHES TO NONLINEAR ADAPTIVE OPTICS AT 1.3μ

A. Elçi and D. Rogovin

Science Applications, Inc.,1200 Prospect Street,La Jolla, CA 92038

bstract

In gases degenerate four-wave mixing at 1.3μ poses unusual difficulties due to the lack of suitable systems. However, nonlinear adaptive optics at these wavelengths appears to be quite promising in solids.

introduction

Recent advances in the technology of the chemically pumped atomic iodine laser have generated an interest in the resonantly enhanced phase conjugation via degenerate four-wave mixing at 1.3μ. Previous studies have shown that the reflectivity of the conjugate waves is sensitive to frequency detuning from an allowed atomic or molecular transition.[1] For instance, the reflectivity for NH_3 is essentially zero a few wavenumbers from an allowed transition.[2] The fact that one needs to work near an allowed transition limits drastically the number and type of materials one can use as conjugators at 1.3μ.Unfortunately, there do not appear to be any known gases which are suitable for resonant degenerate four-wave mixing at 1.3μ, at least not in thermal equilibrium. Althouch resonant 1.3μ-transitions do occur between some excited states in atomic gases, their short T_2 times as well as the additional difficulties due to maintaining the medium in a specified nonequilibrium state make their use impractical. Two-photon resonances and the use of neutral iodine are also impractical as discussed below.However, there are solid-state systems which are quite promising; particularly the following two:

(1) The semiconductor alloy $(Ga_xIn_{1-x})As$ with $x \approx 0.6$,

(2) Atomic or molecular impurities embedded in solid dielectrics.

The following two sections are devoted to the discussion of these two systems. In the remainder of this introduction we discuss briefly the limitations of the use of two-photon resonance and neutral atomic iodine.

To examine the two-photon resonant enhancement of degenerate four-wave mixing in gases, we consider the three-level configurations depicted in Fig. 1. In Configuration A, levels 0 and 2 are not coupled by radiative transitions and $\omega_0 \neq \omega_1 \neq \omega$, but $2\omega = \omega_0 + \omega_1$. If the atom or the molecule is initially in its ground state, then the third-order susceptibility at ω is approximately given by[2]

$$\chi^{(3)}(\omega) = (2\hbar^3)^{-1} N |\mu_{12}|^2 |\mu_{10}|^2 (\omega_0-\omega_1)(\omega-\omega_0+i\gamma)^{-2}(\omega-\omega_1+i\gamma)^{-1}(2\omega-\omega_0-\omega_1+i\gamma)^{-1}. \quad (1)$$

Typically, $\gamma \sim 2\times10^8$ rad.sec^{-1} at 1 torr [3] and $\mu_{12} \sim \mu_{10} \sim 1$ Debye. Let $\omega \sim 1$ eV and $2\omega = \omega_0+\omega_1$, then at one torr,

$$|\chi^{(3)}(\omega)| \sim [6\times10^{-14}\text{esu}].(\omega_0+\omega_1)^2 |\omega_0-\omega_1| [(\omega_0-\omega_1)^2+4\gamma^2]^{-3/2}. \quad (2)$$

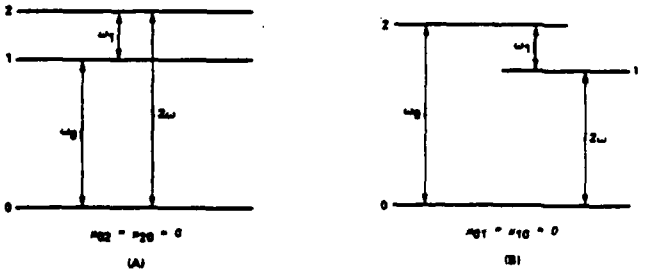

(A) (B)

FIG.1.Two-photon resonance in three-level systems.

The overall frequency factor in Eq.(2) is on the order of unity if ω is significantly different from ω_1. To achieve useful reflectivities, $|\chi^{(3)}|$ should be on the order of 10^{-11} esu or larger. To increase the right hand side of (2) to 10^{-11} esu requires $\omega \sim \omega_1 \sim \omega_0$, in which case single photon transitions are important and Eq.(1) does not apply. Besides, in that case one has found a system whose level structure matches iodine.

In Configuration B, levels 0 and 2, and 1 and 2 are coupled by dipole transitions; 0 and 1 are not. In this case we assume that $2\omega = \omega_0 - \omega_1$; then, at one torr,

$$|\chi^{(3)}| \sim [6\times10^{-14}\text{esu}]\cdot(\omega_0-\omega_1)^2(\omega_0+\omega_1)^{-2}. \qquad (3)$$

This is also about two orders of magnitude smaller than the minimum value needed.

The impracticality of neutral iodine comes from the fact that the lasing levels of atomic iodine are coupled by magnetic dipole transitions[4]. Since magnetic dipole transition rates are smaller than electric dipole transition rates by a factor of $(v/c)^2$, the corresponding susceptibilities are related by

$$\chi_M^{(3)}(\omega) \sim (v/c)^4\, \chi_E^{(3)}(\omega) \quad . \qquad (4)$$

Since $(v/c)\sim 10^{-3}$ for outer electrons, it is clear that one cannot achieve useful reflectivities using atomic iodine.

use of $(Ga_xIn_{1-x})As$

When ω matches the band gap of a direct gap semiconductor, the four-wave mixing is resonantly enhanced. One can exploit this fact for phase conjugation at 1.3μ using $(Ga_xIn_{1-x})As$ alloys. They are direct gap materials[5,6] and the size of the band gap depends on the composition x. To a good approximation one can write

$$E_G(x,T) = g_0(T) + g_1(T)x + g_2(T)x^2 \quad . \qquad (5)$$

At T=300K, g_0=0.36eV, g_1=0.77 eV and g_2=0.31eV. It is therefore possible to make the direct gap as close to 1.3μ as desired, either from above or from below, by a judicious choice of the composition, and thus resonantly enhance $\chi^{(3)}$. Further fine tuning is provided by temperature since g's are temperature dependent.

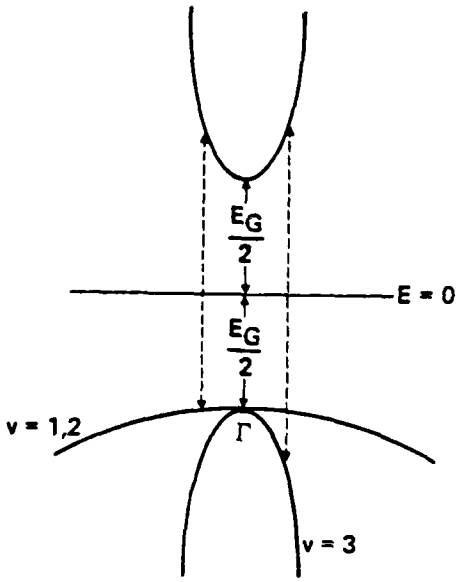

FIG.2. The band structure.

In order to obtain an estimate of the conjugate wave reflectivity, we calculate $\chi^{(3)}$ using the band structure shown in Fig.2 for $(Ga_xIn_{1-x})As$. To simplify the calculation we assume that (a) all waves are polarized in the z-direction; (b) conduction and valence electrons have the same lifetime γ; (c) the dipole moment is given by

$$\vec{L}_{cv} = -ie(m_0E_G\sqrt{\varepsilon_\infty})^{-1}\vec{p}_{cv}(k=0) \quad , \qquad (6)$$

where m_0 is the bare electron mass, ε_∞ is the high frequency dielectric constant and $\vec{p}_{cv}$ is the interband momentum operator; (d) intraband transitions are negligible and only those interband transitions which are near the band gap as shown in Fig.2 need be taken into account; and finally (e) band energies are parabolic:

$$E_c(k) = (E_G/2)+(\hbar^2k^2/2m_\ell),\quad E_v(k)=-(E_G/2)-(\hbar^2k^2/2m_v),\quad m_v=\begin{cases} m_h & \text{for } v=1,2 \\ m_\ell & \text{for } v=3 \end{cases} \quad . \qquad (7)$$

$\chi^{(3)}(\omega=\omega+\omega-\omega)$ is given by (see Ref.2)

$$\chi^{(3)}(\omega) = (2\pi)^{-3}\sum_v \int d\vec{k}\, |L_{cv}|^4 [f(E_v)-f(E_c)]\,[4(L_{vc}-L_{cv})(|L_{vc}|^2+|L_{cv}|^2)+(\hbar\omega+i\gamma/2)^{-1}(L_{cv}^2-L_{vc}^2)], \qquad (8)$$

where $L_{nn'} = (\hbar\omega - E_n + E_{n'} + i\gamma)^{-1}$, $f(E_n) = [1+\exp\beta(E_n - E_f)]^{-1}$, $\beta = (k_B T)^{-1}$, and E_f is the Fermi energy. $\chi^{(3)}$ can be separated into a temperature-independent and a temperature-dependent part. The integrals for the temperature-independent part can be evaluated exactly. Designating the result as $\chi_0^{(3)}$, one finds

$$\chi_0^{(3)}(\omega) = \chi_0\{(\Omega_-/\Delta_-)^{-1}[1+(2\Omega_-/\hbar\omega)+(i\gamma/\Delta_-)+(\Delta_-+i\gamma)(\hbar\omega/2+i\gamma/4)^{-1}] - (\Omega_+/\Delta_+)^{-1}[1+2\Omega_+(\hbar\omega+i\gamma)^{-1}+(i\gamma/\Delta_+)+(\Delta_--i\gamma)(\hbar\omega/2+i\gamma/4)^{-1}]\}, \quad (9)$$

where $\chi_0 = (2\pi\hbar^3)^{-1} \sum_v |\mu_{cv}|^4 (m_\ell m_v)^{3/2} (m_\ell + m_v)^{-3/2}$, $\Omega_\pm = [(E_G \pm \hbar\omega)^2 + \gamma^2]^{1/2}$ and $\Delta_\pm = (E_G \pm \hbar\omega) + \Omega_\pm$.

For small detuning from E_G, $|E_G - \hbar\omega|/E_G \ll 1$, the + terms in (9) can be neglected and

$$\chi_0^{(3)}(\omega) \simeq \chi_0 (\Omega_- \Delta_-^{3/2})^{-1} (\Delta_- - i\gamma). \quad (10)$$

In particular,

$$|\chi_0^{(3)}(\omega)| \simeq \sqrt{2}\chi_0 \Delta_-^{-1/2} = \sqrt{2}\chi_0 [E_G - \hbar\omega + \sqrt{(E_G - \hbar\omega)^2 + \gamma^2}]^{-1/2}. \quad (11)$$

Thus, $|\chi_0^{(3)}|$ rises sharply when ω increases above the band gap as shown in Fig. 3.

The temperature-dependent part of the susceptibility, which we designate as $\chi_t^{(3)}$, cannot be integrated explicitly, although an approximate form for $|E_G - \hbar\omega| \ll E_G$ can be obtained readily. At thermal equilibrium, E_f is nearly in the middle of the gap and thus $E_f \ll E_G$. Using this fact, one finds

$$\chi_t^{(3)}(\omega) \simeq -(1+i)(\pi^2\hbar^3\gamma)^{-1} \sum_v |\mu_{cv}|^4 (2m_\ell m_v)^{3/2} (m_\ell + m_v)^{-3/2} \exp[-\beta(E_G/2 - E_f)] \times \int_0^\infty dy\, y^6 [(y^2 + E_G - \hbar\omega)^2 + \gamma^2]^{-2} \{\exp[-\beta m_v y^2 (m_\ell + m_v)^{-1}] + \exp[-\beta m_\ell m_v y^2 m_h^{-1} (m_\ell + m_v)^{-1}]\} \quad (12)$$

$$\simeq -\frac{15(1+i)(k_B T)^{7/2}[e^{-\beta(E_G/2 - E_f)} - e^{-\beta(E_G/2 + E_f)}]}{4\pi^{3/2}\hbar^3\gamma[(E_G - \hbar\omega)^2 + \gamma^2]^2} \times \sum_v |\mu_{cv}|^4 (m_\ell + m_v)^{1/2} (2m_\ell m_v)^{-1/2} \left(m_\ell^2 + m_h^2\right).$$

In obtaining (12), we neglected $(E_G - \hbar\omega)$ or γ which appear together with y^2 in the numerator, and also used the fact that $\gamma \ll E_G$ or $\hbar\omega$. It is clear from (12) that

$$|\chi_t^{(3)}| / |\chi_0^{(3)}| \sim (k_B T/\gamma)^{7/2} e^{-(\beta E_G/2)}, \quad (13)$$

and thus $\chi_t^{(3)}$ is extremely small compared to $\chi_0^{(3)}$ due to the exponential factor. For all intents, $\chi^{(3)} = \chi_0^{(3)}$.

We can now estimate $\chi^{(3)}$. Let us consider a particular composition with x=0.6 at T=300K, for which $E_G = 0.95$ eV and thus matches 1.3μ. The other parameters are $\varepsilon_r = 10$, $m_\ell = 0.1 m_0$, $m_h = 0.6 m_0$ and $|\mu_{cv}| = 10$ Debye. The finite lifetime for electrons and holes arises mainly from phonon scatterings and is on the order of $\tau = \hbar/\gamma \sim 10^{-12} - 10^{-11}$ sec. Using these values one finds that at 1.3μ, $|\chi^{(3)}| \sim 10^{-7} - 4\times10^{-6}$ esu. These are extremely promising values.

Since both object and conjugate waves are damped in a lossy medium, the reflectivity also depends on absorption even when pump waves are assumed to be undamped. The reflectivity is given by [2]

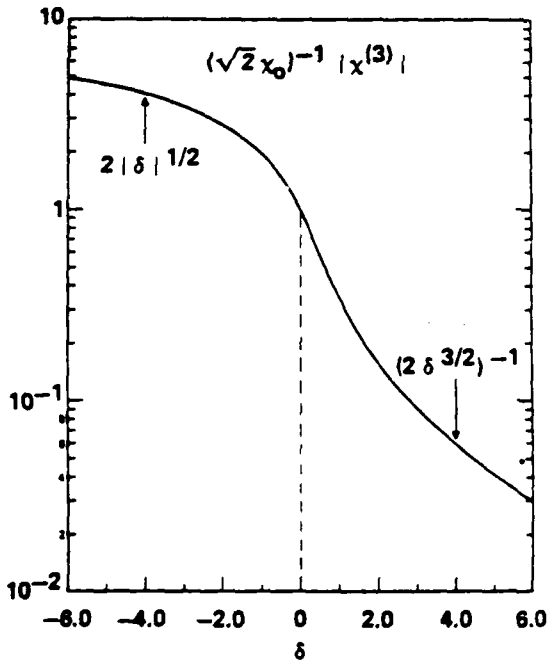

FIG. 3. The third-order susceptibility as a function of the frequency detuning $\delta = (E_G - \hbar\omega)/\gamma$.

$$\eta = |\kappa \sin \xi \ell|^2 |\xi \cos \xi \ell + \alpha \sin \xi \ell|^{-2},$$

$$|\kappa| = 16\pi^2 \omega c^{-2} n_0^{-2} \sqrt{I_1 I_2}\, |\chi^{(3)}|, \tag{14}$$

$$\xi = \sqrt{|\kappa|^2 - \alpha^2},$$

where ℓ is the length of the nonlinear mixing region, n_0 is the index of the refraction, I_1 and I_2 are the intensities of the two counterpropagating pump waves, α is the absorption coefficient. At room temperatures α can be written approximately as [7]

$$\alpha = \begin{cases} \alpha_0 - \alpha_1 (E_G - \hbar\omega) & \text{for } \hbar\omega < E_G \\ \alpha_2 \sqrt{\hbar\omega - E_G} & \text{for } \hbar\omega > E_G \end{cases} \tag{15}$$

where $\alpha_0 = 1.3 \times 10^3$ cm^{-1}, $\alpha_1 = 10^4$ cm^{-1}eV^{-1} and $\alpha_2 = 6 \times 10^3$ cm^{-1} eV$^{-1/2}$. It is clear that absorption will be high and one will usually be in the absorptive regime, i.e. ξ will usually be imaginary. Let $|\chi^{(3)}| = 10^{-6}$ esu and $I_1 = I_2 = 1$ MW/cm^2, then $|\kappa| = 260$ cm^{-1}. α is about 10^3 cm^{-1}. When ξ is imaginary η is independent of ℓ^2 and is given by

$$\eta \approx |\kappa|^2/(2\alpha)^2 = 2 \times 10^{-2} = 2\% \tag{16}$$

This corresponds to a reasonably efficient phase conjugation.

impurities embedded in solid dielectrics

It is clear from the above discussion that if their linewidths were smaller, solids would be extremely efficient for four-wave mixing. One approach for achieving narrow linewidths in solids is to use discrete states which couple weakly to phonons compared to continuum states of the energy bands. For example, when an atom or an ion is embedded in a dielectric, the lifetimes of the low lying states are usually on the order of 10^{-8} sec. One can also use the fact the atomic energy levels are reduced approximately by a factor ε_0^{-2}, where ε_0 is the static dielectric constant, to tune some atomic transition frequencies to 1.3μ by choosing ε_0 appropriately.

For the sake of concreteness we consider alkali type ions embedded in semiconductors and insulators in the following. However, the basic idea can be extended to neutral atoms and other types of ions in highly degenerate solids or glasses. Also, the system whose discrete states are to be used need not be an ion or atom; it could equally well be a defect in the solid.

The discrete energy levels of an alkali ion can be approximated by [8]

$$E_n = E_G - R(Z - Z' + 1)^2 \varepsilon_0^{-2} (n - \Delta)^{-2} \tag{17}$$

where R is the Rydberg energy, Z is the nuclear charge, Z' is the number of electrons, n is an integer and Δ is the quantum defect. The energy levels are measured from the edge of the valence bands. For resonant tuning we require $1.3\mu = \hbar\omega = 0.95\text{eV} = E_{n'} - E_n$, for some $n' > n$. Thus,

$$0.07\varepsilon_0^2 = (Z - Z' + 1)^2 [(n - \Delta)^{-2} - (n' - \Delta)^{-2}]. \tag{18}$$

One way to proceed is to choose a specific atom or ion, as well as a particular transition and then solve for ε_0:

$$\varepsilon_0 = 3.8(Z - Z' + 1) |n' - \Delta|^{-1} |n - \Delta|^{-1} (n' - n)^{1/2} (n + n' - 2\Delta)^{1/2}. \tag{19}$$

Below we list the values of ε_0 given by Eq. (19) for a number of ions. [8]

	n	n'	ε_0
Na^+: $Z-Z'+l=2$, $\Delta=1.4$	1	2	12
	1	∞	19
	2	3	12
	2	∞	13
Al^{+++}: $Z-Z'+l=4$, $\Delta=0.9$	1	2	68
	1	∞	152
P^{5+}: $Z-Z'+l=6$, $\Delta=0.7$	1	2	99
	1	∞	76

As static dielectric constants go, all of these are reasonable values. In small gap materials ($E_G \lesssim 0.2$eV) ε_0 is usually large. For insulator and high gap materials ε_0 is on the order of 10.

At first glance, it may seem that there would be strong absorption in small gap materials like PbSe or PbTe alloys, since $\hbar\omega > E_G$ and thus they would have negligible reflectivity. However, 1eV is so large compared to the gaps of these materials that the transition would fall onto very high conduction bands. By a slight adjustment of the composition, the relative position of these bands can be altered and absorption decreased. ε_0 can also be adjusted by varying the alloy composition.

The numbers for Na^+ are quite close to pure Si and CdS. Si has $\varepsilon_0 \approx 11.8$. CdS is an insulator and has $E_G \approx 2.4$eV. CdS has an added advantage in that absorption at 1.3μ would only be due to the impurity sites themselves, and hence these transitions can be saturated for sufficiently low impurity densities.

We acknowledge the support of AFOSR for this work.

references

1. A. Elçi and D. Rogovin, Opt. Letts., 5(1980)255.
2. A. Elçi et al., J. Opt. Soc. Am., 70(1980)990.
3. This value corresponds to the pressure-broadened linewidth of NH_3 at 1 torr.
4. V. S. Zuev, et al., Soviet Physics JETP 35(1972)870.
5. D. Long, "Energy band structures of mixed crystals of III-V compounds", in Semiconductors and Semimetals, Vol. I, Eds. R.K. Willardson and A.C.Beer (Academic Press, New York 1966).
6. These compounds can lase at 1.3μ. There is a great deal of literature on the subject. See, for example, R.J. Nelson, et al., Appl. Phys. Letts. 36(5)(1980)358 and 36(7)(1980)518; J.N. Walpole, et al., Appl. Phys. Letts. 36(4)(1980)240; K. Takahei, et al., Appl. Phys. Letts. 36(4)(1980)309.
7. These values are extrapolated from those of GaAs, for which see T.S. Moss, G.J. Burrell and B. Ellis, Semiconductor Opto-electronics (Butterworth & Co., London 1973).
8. M. Mizushima, Quantum Mechanics of Atomic Spectra and Atomic Structure (W.A. Benjamin, Inc., New York 1970).

APPENDIX 2

FOUR-WAVE MIXING AND PHASE CONJUGATION NEAR THE BAND EDGE

by

A. Elci and D. Rogovin

FOUR-WAVE MIXING AND PHASE CONJUGATION NEAR THE BAND EDGE

By

A. Elci and D. Rogovin

Science Applications, Inc.
1200 Prospect Street
La Jolla, CA 92038

ABSTRACT

We discuss degenerate four-wave mixing and phase conjugation near the band edge of direct gap semiconductors and show that the reflectivity for conjugate waves is resonantly enhanced in the vicinity of the band edge. We also compare the quantum mechanical results with the classical Drude model.

I. INTRODUCTION

There is presently a considerable body of work on phase conjugation via degenerate four-wave mixing in semiconductors.[1-6] It has been motivated partly by the availability of a variety of frequency ranges, and partly by the relatively high efficiencies observed in these materials. This paper, too, is concerned with degenerate four-wave mixing. We consider a direct gap semiconductor and calculate the contribution of interband transitions near the band edge to the third order susceptibility $\chi^{(3)}(\omega = \omega + \omega - \omega)$. We also consider the absorption coefficient α in the semiconductor in order to obtain a realistic expression for the conjugate wave reflectivity η.

There are two reasons for the interest in a band-edge mechanism for four-wave mixing. First, $\chi^{(3)}$ is resonantly enhanced as $\hbar\omega$ increases to E_G, the band gap. As a result, η is also enhanced despite increased absorption (which adversely affects phase conjugation[7,8]). Second, a band-edge mechanism offers a greater potential for frequency tunability, since in many semiconductor compounds such as $Ga_{1-x}(InAs)_x$, $Cd_{1-x}(HgTe)_x$, $Pb_{1-x}(SnSe)_x$, etc., E_G can be continuously varied by changing composition.[9]

A number of authors have discussed band-edge mechanisms for four-wave mixing.[1,3,6] Among these, R. K. Jain, et al.,[1,3] have considered a mechanism which is similar to what we have in mind. They imagine creation of an electron-hole plasma in the semiconductor and use a Drude model to calculate $\chi^{(3)}$. In this paper, however, we perform a density matrix calculation to provide a more precise picture of the frequency dependence of

$\chi^{(3)}$ and η. Also, our results apply to frequencies that are lower than E_G. A detailed comparison of our results with those of Ref. 1 is given in Section V. Finally, we also note that M. A. Khan, et al.,[4] have studied a case in which $\chi^{(3)}$ is resonant for $\hbar\omega \sim E_G$ because of a nonparabolic band structure. This nonlinear process is quite different than the one taken up here.[10] Here, we are concerned with an ordinary and direct electron-field coupling via interband transitions.

In Section II, we describe the band structure used in the calculation. It is a simplified version of the band structure of III-V compounds, chosen with the phase conjugation of iodine laser beams in mind. In Section III we give the general results for a two-component plasma in the semiconductor. In Section IV, the general results are specialized to small perturbations from thermal equilibrium. Finally, in Section VI, we discuss the reflectivity of a spacific direct gap semiconductor, $Ga_{1-x}(InAs)_x$.

The main result of our work is that the reflectivity of conjugate waves has a resonance in the vicinity of the band edge. The precise position of the resonance depends parametrically on the sample thickness. The resonance shifts to lower frequencies for thicker samples, as one might expect from the depletion of the pump waves. If the depletion of the pump waves are negligible, as when the semiconductor is saturated, then the reflectivity is nearly constant above the band edge and decreases rapidly below it, independently of the sample thickness.

II. BAND MODEL

To be definite, we assume a band structure as shown in Fig. 1, which is typical of III-V compounds. It has one light hole band, two heavy hole bands which are degenerate, and one conduction band. To simplify the calculation we also assume that the bands are parabolic:

$$E_c(\vec{k}) = (E_G/2) + (\hbar^2 k^2/2m_c^*) \tag{1a}$$

$$E_v(\vec{k}) = -(E_G/2) - (\hbar^2 k^2/2m_v^*), \quad (v=1,2,3) , \tag{1b}$$

where the m*'s are the appropriate effective masses near the center of the Brillouin Zone. For the calculation one also needs the dipole matrix element for the interband transitions. It is related to the more familiar interband momentum matrix element by the following relations:

$$\vec{D} = -e\varepsilon_\infty^{-1/2}\vec{x} , \tag{2a}$$

$$\vec{p} = -im_0\hbar^{-1}\left[\vec{x}, H_0\right] , \tag{2b}$$

$$\vec{D}_{cv} = -ie\hbar m_0^{-1}\varepsilon_\infty^{-1/2}\left(E_c - E_v\right)^{-1}\vec{p}_{cv} \tag{2c}$$

Here ε_∞ is the high frequency dielectric constant, m_0 is the bare electron mass, and H_0 is the one-electron crystal Hamiltonian. The factor $\varepsilon_\infty^{-1/2}$ in (2a) comes from high frequency screening of electrons and renormalizes the bare electronic charge. Since our concern is with the band edge, the

right hand side of (2c) need be evaluated only at $\vec{k}=0$. $\vec{\mu}_{cv}$ can be taken as constant.

We are interested in those situations in which the semiconductor is either at room temperature or at a temperature which is not too low relative to room temperature. At these temperatures the absorption edge is smoothly broadened to frequencies which are considerably below the band edge, due to interactions among electrons, holes and phonons. To take into account this broadening, we assign average linewidths γ_c and γ_v to electron and hole states, respectively. This procedure should be adequate to describe the actual situation for intermediate and room temperatures. However, for lower temperatures, there are well defined discrete excitonic peaks and one must take the discrete nature of these peaks into account. This requires considerable modification of the calculation and is reserved for another publication. Here we confine ourselves to the regime in which discrete excitonic peaks are not observable.

III. THIRD ORDER SUSCEPTIBILITY, ABSORPTION AND REFLECTIVITY

The geometry of degenerate four-wave mixing is shown in Fig. 2. We assume that all four waves are linearly polarized in the z-direction and actually calculate $\chi^{(3)}_{zzzz}$ ($\omega = \omega + \omega - \omega$). Since absorption is important for phase conjugation, we also calculate the frequency-dependent absorption coefficient $\alpha(\omega)$ under the same assumptions. A density matrix calculation gives the following expressions for $\chi^{(3)}$ and α (see Ref. 8 and Footnote 11):

$$\chi^{(3)} = \sum_{v=1}^{3} \int_{BZ} d\vec{k}(2\pi)^{-3}|\mu^z_{cv}|^4\left[f(E_v) - f(E_c)\right] \tag{3a}$$

$$\times \left[(\gamma_c+\gamma_v)^2(\gamma_c\gamma_v)^{-1}(L_{vc}-L_{cv})(|L_{vc}|^2 + |L_{cv}|^2)\right.$$

$$\left. + (4\hbar\omega+i\gamma_c+i\gamma_v)(2\hbar\omega+i\gamma_c)^{-1}(2\hbar\omega+i\gamma_v)^{-1}(L^2_{cv}-L^2_{vc})\right] ,$$

$$\alpha = \hbar n\omega^2(c\pi^2E_G)^{-1} \sum_{v=1}^{3} \gamma_{cv}|\mu^z_{cv}|^2 \int_{BZ} d\vec{k}\left[f(E_v)-f(E_c)\right] \tag{3b}$$

$$\times \left[|L_{cv}|^2 + |L_{vc}|^2\right]$$

where $n = \sqrt{\varepsilon_\infty}$ is the index of refraction, and

$$L_{nn'} = \left[\hbar\omega - E_n(\vec{k}) + E_{n'}(\vec{k}) + i\gamma_{nn'}\right]^{-1} , \tag{4a}$$

$$\gamma_{nn'} = (\gamma_n+\gamma_{n'})/2 , \tag{4b}$$

$$f(E_n) = \left[1 + \exp\beta(E_n(\vec{k})-E_{fn})\right]^{-1} , \ \beta = (k_BT)^{-1} , \tag{4c}$$

$$E_{fn} = \begin{cases} E_{fc} & \text{for } n=c \\ -E_{fh} & \text{for } n=v=1,2,3 . \end{cases} \tag{4d}$$

In (4c,d), E_{fn} are Fermi energies for electrons and holes, assumed to be distinct in order to include those situations in which absorption at $\hbar\omega$ significantly affects band populations.[12]

One can let the upper limit of k go to infinity to simplify the integrals. We do not expect much error resulting from this procedure since as $k \to \infty$, the integrands decrease rapidly for parabolic bands. However, the situation is quite different for nonparabolic bands. For instance, the integrals for Kane's two-band model[13] diverge if one lets the upper limit of k go to infinity; therefore, they must be evaluated for a finite Brillouin Zone.

$\chi^{(3)}$ and α consist of two types of terms,

$$\chi^{(3)} = \sum_{v=1}^{3} (K_v^o + K_v^t), \tag{5a}$$

$$\alpha = \sum_{v=1}^{3} (A_v^o + A_v^t), \tag{5b}$$

where K_v^o and A_v^o are temperature independent, and K_v^t and A_v^t are temperature dependent. This separation is effected by writing the population factor as

$$\begin{aligned} f(E_v) - f(E_c) &= 1 - [1 - f(E_v) + f(E_c)] \\ &= 1 - \left\{[1 + \exp\beta(-E_v - E_{fh})]^{-1} + [1 + \exp\beta(E_c - E_{fc})]^{-1}\right\}. \end{aligned} \tag{6}$$

The integrals for K_v^o and A_v^o can be evaluated by contour integration (see the appendix) and one finds

$$K_v^o = (2\pi)^{-1}\hbar^{-3}m_v^{3/2}|\mu_{cv}^z|^4\left\{\left[2\gamma_{cv}^2(\gamma_c\gamma_v\hbar\omega\sqrt{\Delta_-})^{-1}\right]\right. \tag{7a}$$

$$+\left[(\Delta_-+i\gamma_{cv})(\Omega_-\sqrt{\Delta_-})^{-1}\right]\left[\gamma_{cv}^2(\Delta_-\gamma_c\gamma_v)^{-1}+(4\hbar\omega+2i\gamma_c)^{-1}+(4\hbar\omega+2i\gamma_v)^{-1}\right]$$

$$+\left[(\Delta_+-i\gamma_{cv})(\Omega_+\sqrt{\Delta_+})^{-1}\right]\left[\gamma_{cv}^2(\Delta_+\gamma_c\gamma_v)^{-1}-(4\hbar\omega+2i\gamma_c)^{-1}-(4\hbar\omega+2i\gamma_v)^{-1}\right]$$

$$\left.-\left[2\gamma_{cv}^2(\gamma_c\gamma_v\hbar\omega\sqrt{\Delta_+})^{-1}\right]\right\}$$

and

$$A_v^o = 4n\omega^2 m_v^{3/2}|\mu_{cv}^z|^2(\hbar^2 cE_G)^{-1}\left[\Delta_-+2(\hbar\omega-E_G)\right]^{1/2}\ , \tag{7b}$$

where

$$m_v = m_c^* m_v^*(m_c^*+m_v^*)^{-1}\ , \tag{7c}$$

$$\Omega_\pm = \left[(E_G\pm\hbar\omega)^2 + \gamma_{cv}^2\right]^{1/2}\ , \tag{7d}$$

and

$$\Delta_\pm = \Omega_\pm + (E_G\pm\hbar\omega)\ . \tag{7e}$$

The temperature-dependent terms cannot be evaluated explicitly for arbitrary temperature. We write them in terms of Fermi-Dirac integrals of the dimensionless form

$$F_m^n(j;a) = \int_o^\infty dy\ y^n(y^2+a)^{-m}\left[1+c_j\ \exp\left(b_j y^2\right)\right]^{-1}\ . \tag{8}$$

Let us define

$$\zeta = (E_G+i\gamma_{cv})/\hbar\omega\ , \tag{9a}$$

$$c_1 = \exp\beta\left(E_G/2-E_{fc}\right)\ , \tag{9b}$$

$$c_2 = \exp\beta\left(E_G/2-E_{fh}\right)\ , \tag{9c}$$

$$b_1 = (m_v/m_c^*)\,\beta\hbar\omega\ , \tag{9d}$$

$$b_2 = (m_v/m_v^*)\,\beta\hbar\omega\ . \tag{9e}$$

K_v^t and A_v^t are then given by

$$K_v^t = (\pi^2\hbar^3\gamma_c\gamma_v)^{-1}(2m_v)^{3/2}(\hbar\omega)^{1/2}|\mu_{cv}^z|^4 \tag{10a}$$

$$\times \sum_{j=1}^{2}\Big\{\mathrm{Im}\Big[F_1^2(j;\zeta-1) + F_1^2(j;\zeta^*+1)\Big]$$

$$+ i(\gamma_{cv}/\hbar\omega)\Big[F_2^2(j;\zeta^*-1) - F_2^2(j;\zeta+1)\Big]$$

$$+ (\gamma_{cv}/\hbar\omega)\mathrm{Re}\Big[i(\zeta-1)F_1^0(j;\zeta-1) + i(\zeta^*+1)F_1^0(j;\zeta^*+1)\Big]$$

$$+ (\gamma_c\gamma_v/2\hbar\omega)\Big[(2\hbar\omega+i\gamma_c)^{-1} + (2\hbar\omega+i\gamma_v)^{-1}\Big]\Big[F_2^2(j;\zeta+1) - F_2^2(j;\zeta^*-1)\Big]\Big\}$$

and

$$A_v^t = 4\omega n|\mu_{cv}^z|^2(2m_v\omega/\hbar)^{3/2}(\pi cE_G)^{-1}\sum_{j=1}^{2}\mathrm{Im}\Big[F_1^2(j;\zeta-1) + F_1^2(j;\zeta+1)\Big]. \tag{10b}$$

Finally, the reflectivity for conjugate waves in degenerate four-wave mixing is given by[7,8]

$$\eta = |\kappa\sin\xi\ell|^2|\xi\cos\xi\ell + \alpha\sin\xi\ell|^{-2} \quad , \tag{11a}$$

where

$$|\kappa| = 16\pi^2\omega c^{-2}\varepsilon_\infty^{-1}(I_1I_2)^{1/2}|\chi^{(3)}| \tag{11b}$$

and

$$\xi = (|\kappa|^2 - \alpha^2)^{1/2} \quad . \tag{11c}$$

In Eq. (11a), ℓ is the length of the nonlinear mixing region, and I_1 and I_2 are the intensities of the two counterpropagating pump waves. We note that (11a) is derived under the assumption that the conjugate and signal

waves are depleted but the pump waves are not. When the depletion of the pump waves is also taken into account, as seen from Fig. 2, the constant pump amplitudes A_1 and A_2 are replaced by

$$A_1(x) = A_1(\ell) \exp\ [-(\ell-x)\alpha/2] , \tag{11d}$$

$$A_2(x) = A_2(o) \exp\ (-\alpha x/2) , \tag{11e}$$

and thus the product

$$A_1(x)A_2(x) = A_1(\ell)A_2(o) \exp\ (-\alpha\ell/2) \tag{11f}$$

is independent of position. $|\kappa|$ becomes

$$|\kappa| = 16\pi^2\omega c^{-2}\varepsilon_\infty^{-1}(I_1I_2)^{1/2}|\chi^{(3)}|\exp\ (-\alpha\ell/2) . \tag{11g}$$

Above the band edge α is usually on the order of 10^4 cm^{-1}. All four waves can be severely depleted and one should use (11g). The use of (11b) should be restricted to frequencies that are lower than the band edge. There is still significant absorption at these frequencies, however, due to the broadening of the absorption edge.

IV. MODERATE EXCITATIONS

In order to obtain efficient phase conjugation, one would naturally seek a situation in which absorption at $\hbar\omega$ is as low as possible. We now take this to be the case and assume that electron and hole populations are not perturbed significantly from their equilibrium forms. We note in passing that this assumption contrasts with the premise of Ref. 1 in which Jain and Klein imagine creation of a dense electron-hole plasma in the semiconductor. In their case, it would be more appropriate to assign a separate Fermi energy to each component of the plasma, since each thermalizes separately before the interband transitions can take over and bring the two components into a common thermal equilibrium.[12]

At the thermal equilibrium, there is one common Fermi energy:

$$E_f = E_{fc} = -E_{fh} \tag{12a}$$

E_f is nearly in the middle of the band gap, given by

$$E_f \simeq (k_B T/2) \ell n \left[1 + \sum_v (m_v^*/m_c^*)^{3/2} \right] . \tag{12b}$$

One can therefore set

$$c_1 \simeq c_2 \simeq \exp(\beta E_G/2) >> 1 \tag{13}$$

for band gaps on the order of 0.5-1 eV and for room temperatures. Also, the integrand in (8) contributes mostly in the vicinity of y=0 and

$$F_m^n(j;a) \approx (2c_j)^{-l_a - m_{b_j} - (\frac{n+1}{2})} \Gamma(\frac{n+1}{2}) . \tag{14}$$

To simplify the following discussion, we further assume that $\gamma_c = \gamma_v = \gamma$ and focus our attention on the vicinity of the band edge, by which we mean $|E_G - \hbar\omega|/E_G << 1$.

In the vicinity of the band edge (7a) yields

$$\sum_v K_v^o = \chi_o\left[i+\delta+\sqrt{1+\delta^2}\right]\left[\delta+\sqrt{1+\delta^2}\right]^{-3/2}\ (1+\delta^2)^{-1/2}\ , \tag{15a}$$

where

$$\delta = (E_G - \hbar\omega)/\gamma \tag{15b}$$

and

$$\chi_o = (2\pi\hbar^3\gamma^{3/2})^{-1} \sum_v m_v^{3/2}|\mu_{cv}^z|^4\ . \tag{15c}$$

From (7b), one has

$$\sum_v A_v^o = \alpha_o\left[\sqrt{1+\delta^2}\ -\delta\right]^{1/2}\ , \tag{16a}$$

where

$$\alpha_o = 4\pi\omega^2\gamma^{1/2}(\hbar^2 c E_G)^{-1} \sum_v m_v^{3/2}|\mu_{cv}^z|^2\ . \tag{16b}$$

Similarly, the use of (14) in the vicinity of the band edge yields

$$\sum_v K_v^t = \chi_t(\delta+1)(\delta+i)(1+\delta^2)^{-2} \tag{17a}$$

and

$$\sum_v A_v^t = \alpha_t(1+\delta^2)^{-2}\ , \tag{17b}$$

where

$$\chi_t = 2(i-1)(2\pi\beta)^{-3/2}\hbar^{-3}\gamma^{-3}\exp(-\beta E_G/2)\sum_v|\mu_{cv}^z|^4\left[(m_c^*)^{3/2}+(m_v^*)^{3/2}\right] \tag{17c}$$

and

$$\alpha_t = -4n(2\pi\hbar)^{-1/2}(cE_G\gamma)^{-1}\omega^{7/2}\exp(-\beta E_G/2)\sum_v|\mu_{cv}^z|^2\left[(m_c^*)^{3/2}+(m_v^*)^{3/2}\right] . \tag{17d}$$

We can now compare temperature-dependent and temperature-independent terms. From (15c), (16b), (17c) and (17d), one finds

$$|\chi_t/\chi_o| \sim (2\pi)(k_BT/\pi\gamma)^{3/2}\exp(-\beta E_G/2) \tag{18a}$$

and

$$|\alpha_t/\alpha_o| \sim (2\pi)(\hbar\omega/2\pi\gamma)^{3/2}\exp(-\beta E_G/2) \quad . \tag{18b}$$

Due to the exponential terms, the temperature-dependent terms are clearly negligible either for room temperatures under thermal equilibrium conditions, or for small perturbations from thermal equilibrium. For lower temperatures they decrease further, exponentially. For all intents and purposes, $\chi^{(3)}$ and α are given by the temperature-independent terms under moderate excitations as long as the band gap is not too small.

Neglecting the temperature-dependent terms,

$$\alpha = \alpha_o\left[\sqrt{1+\delta^2} - \delta\right]^{1/2} \tag{19a}$$

$$= \alpha_o\left[\sqrt{1+\delta^2} + \delta\right]^{-1/2} , \tag{19b}$$

$$\mathrm{Re}\chi^{(3)} = (\chi_o/\alpha_o)(1+\delta^2)^{-1/2}\,\alpha \tag{19c}$$

$$= 2\alpha_o\chi_o\alpha^3\left[\alpha_o^4 + \alpha^4\right]^{-1} , \tag{19d}$$

and

$$\mathrm{Im}\chi^{(3)} = (\chi_o/\alpha_o^3)(1+\delta^2)^{1/2}\,\alpha^3 \tag{19e}$$

$$= (2\chi_o/\alpha_o)\alpha^5\left[\alpha_o^4 + \alpha^4\right]^{-1} . \tag{19f}$$

Finally one needs $|\chi^{(3)}|$ for the reflectivity:

$$|\chi^{(3)}| = \sqrt{2}\,\chi_o(1+\delta^2)^{-1/4}(\sqrt{1+\delta^2} + \delta)^{-1} . \tag{19g}$$

Fig. 3 shows $|\chi^{(3)}|/(\sqrt{2}\chi_o)$ as a function of $\delta = (E_G - \hbar\omega)\gamma^{-1}$, the frequency detuning per linewidth. Below the band gap, $\delta >> 1$ and

$$|\chi^{(3)}| \simeq 2\chi_o(2\delta)^{-3/2} , \tag{20a}$$

which should be compared with

$$\alpha \simeq \alpha_o(2\delta)^{-1} \tag{20b}$$

in the same region. Thus, $|\chi^{(3)}|$ decreases faster compared to α for $\delta > 1$. Above the band gap, $\delta < o$, $|\delta| >> 1$, and

$$|\chi^{(3)}| \simeq 2\chi_o(2\delta)^{1/2} , \tag{20c}$$

which has the same δ-dependence as α.

V. COMPARISON WITH DRUDE MODEL

We can compare our expression for $\chi^{(3)}$ with that of Jain and Klein[1]. Their expression for $\chi^{(3)}$, obtained from a Drude model, is

$$\chi_D^{(3)} = nce^2\tau\eta^*\alpha^*(8\pi m^*_{eh}\hbar\omega^3)^{-1} \tag{21}$$

Here τ is the lifetime for electrons and holes, α^* is the total absorption coefficient, $(\eta^*\alpha^*)$ designates the fraction of the absorption which corresponds to an actual electron-hole pair creation (i.e., $\eta^*\alpha^*$ corresponds to our α), and m^*_{eh} is the reduced mass of an electron and a hole: $m^*_{eh} = m^*_e\, m^*_h\, (m^*_e + m^*_h)^{-1}$. $\chi_D^{(3)}$ is real and describes an adiabatic response of the system. It corresponds to our $\mathrm{Re}\chi^{(3)}$. Our expression for $\chi^{(3)}$ has an additional part which is imaginary. $\mathrm{Im}\,\chi^{(3)}$ describes those processes in which at least one real transition occurs. Such processes can either put energy into the system or extract energy from the system. Note that above the band edge, $\delta<0$ and $|\delta|>>1$. One therefore has $\alpha>>\alpha_o$, and (19f) simplifies to

$$\mathrm{Im}\chi^{(3)} \simeq (2\chi_o/\alpha_o)\alpha \tag{22}$$

Thus, above the band edge $\mathrm{Im}\chi^{(3)}$ is proportional to the absorption coefficient, having the same functional dependence on the frequency detuning $(E_G-\hbar\omega)$ as α. This is consistent with having at least one real transition occur.

To compare $\chi_D^{(3)}$ and $\mathrm{Re}\chi^{(3)}$, we make the following approximations. The ratio of the sums over the dipole moments can be estimated as

$$\left(\sum_v m_v^{3/2}|\mu_{cv}^z|^4\right)\left(\sum_v m_v^{3/2}|\mu_{cv}^z|^2\right)^{-1} \approx |\mu_{c1}^z|^2 \quad . \tag{23a}$$

Using (2c), one has

$$|\mu_{c1}^z|^2 = e^2\hbar^2|p_{c1}^z|^2(m_o^2n^2E_G^2)^{-1} \quad . \tag{23b}$$

The momentum matrix element is related to the electron and hole masses near the band edge (see Ref. 12):

$$|p_{c1}^z|^2(m_o^2E_G)^{-1} \approx (2m_{eh}^*)^{-1} \quad . \tag{24}$$

With these approximations and also using $\gamma = (\hbar/\tau)$, one finds

$$\mathrm{Re}\chi^{(3)} \approx (\hbar\omega/2)\left[(\hbar\omega-E_G)^2 + \gamma^2\right]^{-1/2} n^{-4}\chi_D^{(3)} \quad . \tag{25}$$

Thus, as far as the frequency dependence is concerned, the two expressions differ only by the square root of a Lorentz factor. The other factor n^{-4} arises from two sources. One is that we are taking into account the short wavelength screening and treating electrons as particles each with an effective charge $e/\sqrt{\varepsilon_\infty} = e/n$, as in (2a). This contributes a factor n^{-2} in (25). The remaining n^{-2} factor comes from the difference between the way we count the number of photons and the way it is done in Ref. 1. We

use the standard expansion for the electric field operator such that (see Ref. 14),

$$\vec{E}(\vec{x},t) = \sum_{\lambda} i(2\pi\hbar\omega_\lambda/V)^{1/2}\,\hat{e}_\lambda\left\{b_\lambda \exp\left[i(\vec{k}_\lambda\cdot\vec{x}-\omega_\lambda t)\right]-b_\lambda^{+}\exp\left[-i(\vec{k}_\lambda\cdot\vec{x}-\omega_\lambda t)\right]\right\}, \tag{26a}$$

with

$$\left[b_\lambda, b_{\lambda'}^{+}\right] = \delta_{\lambda\lambda'} , \tag{26b}$$

where λ designates the modes, $\hat{e}_\lambda$ is the unit polarization vector, V is the volume, and ω_λ and k_λ are related by

$$\omega_\lambda = (c/n)k_\lambda . \tag{26c}$$

For a single coherent mode at ω,

$$(4\pi)^{-1}\int d\vec{x}\,\langle\vec{E}^2\rangle_\omega = \hbar\omega\langle b^{+}b\rangle \approx \hbar\omega N , \tag{27}$$

where N is the average number of photons in this mode. Thus, the photon *current* density is

$$j_\gamma = c\langle\vec{E}^2\rangle_\omega(4\pi\hbar\omega n)^{-1} . \tag{28}$$

For complex field amplitudes,

$$j_\gamma = c\langle\vec{E}\cdot\vec{E}^{*}\rangle_\omega(8\pi\hbar\omega n)^{-1} . \tag{29}$$

This expression for j_γ differs from the corresponding one in Ref. 1 in that (29) has an extra n^{-2} factor. Finally, if we write out $n^{-4}\chi_D^{(3)}$,

$$n^{-4}\chi_D^{(3)} = (c/n)(e^2/\varepsilon_\infty)(\tau\eta^{*}\alpha^{*})(8\pi m_{eh}^{*}\,\hbar\omega^3)^{-1} , \tag{30}$$

we see that n^{-4} factor helps to renormalize both the charge and the speed of light.

It is interesting that the presence of n^{-4} somewhat compensates for the Lorentz factor in (25) and makes $\mathrm{Re}\chi^{(3)}$ and $\chi_D^{(3)}$ comparable, since usually $n^2 \sim$ 10-20 for semiconductors.

VI. REFLECTIVITY FOR $Ga_{1-x}(InAs)_x$

We now consider a specific semiconductor: $Ga_{1-x}(InAs)_x$ with $x \simeq 0.4$ for which the band gap is $E_G \simeq 0.95$ eV. This coice is motivated by the fact that $\lambda_o = 2\pi\hbar c E_G^{-1} \simeq 1.3$ μm, which coincides with the wavelength of high energy iodine lasers. There has been a practical interest in obtaining phase conjugation at the iodine wavelength. To the authors' knowledge there is no gaseous or atomic system which matches this wavelength and which might be used for resonant enhancement of the conjugation process. Neutral iodine itself cannot be used, since the lasing transition is a magnetic dipole transition. A semiconductor such as $Ga_{1-x}(InAs)_x$ is therefore a natural choice for phase conjugation at $\lambda_o = 1.3$ μm.

The remaining parameters for our sample are $\varepsilon_\infty \simeq 10$, $m_c^* = m_3^* \simeq 0.1\ m_o$ and $m_1^* = m_2^* \simeq 0.6\ m_o$ (see Ref. 15). A typical lifetime is $\tau = (\hbar/\gamma) \simeq 10^{-11}$ sec^{-1}. Thus,

$$m_{eh}^* = m_c^* m_1^* (m_c^* + m_1^*)^{-1} \simeq 0.09\ m_o \tag{31a}$$

and

$$|\mu_{c1}^z| \simeq e\hbar(2m_{eh}^* \varepsilon_\infty E_G)^{-1} \simeq 10 \text{ Debye}, \tag{31b}$$

where we used (23b) and (24). Setting $E_G \simeq \hbar\omega$ in (15c) and (16b) yields $\chi_o \simeq 3 \times 10^{-6}$esu and $\alpha_o \simeq 1.2 \times 10^3$ cm^{-1}. The value of α_o, which corresponds to the value of α at the exact band edge $\xi = (E_G - \hbar\omega)/\gamma = 0$, is in reasonable agreement with the experimentally observed value for GaAs (see

page 61 of Ref. 15). Further, let $I_1=I_2=1MW/cm^2$, then from (11b), $|\kappa| \approx 1.1 \times 10^3\ cm^{-1}$, which is comparable to but less than α. Two comments are in order. The first is that $|\chi^{(3)}|$ and hence $|\kappa|$ are quite sensitive to the linewidth. For example, for $\tau = 10^{-12}\ sec^{-1}$, one finds $\alpha_0 \approx 4 \times 10^3\ cm^{-1}$, $\chi_0 \approx 10^{-7}$ esu and $|\kappa| \approx 36\ cm^{-1}$. The second is that the parameter ξ of (11c), which actually determines the reflectivity, is usually an imaginary quantity. For imaginary ξ, (11a) simplifies to

$$\eta = |\kappa|^2(2\alpha)^{-2} \ . \tag{32}$$

Thus, if the pump waves are not depleted and $\tau = 10^{-11}\ sec^{-1}$, one has from (32) and (11b) that $\eta \approx 0.22 = 22\%$, which is a reasonably efficient phase conjugation.

The frequency-detuning dependence of η as given by (32) can be written out as

$$\eta = \eta_0(1+\delta^2)^{-1/2}(\sqrt{1+\delta^2}-\delta)\ \exp\left[-\sigma_0(\sqrt{1+\delta^2}-\delta)^{1/2}\right], \tag{33a}$$

where

$$\eta_0 = 2\pi^2 E_G^2(\hbar^2\omega^2c^2\gamma^4n^6)^{-1}(\sum_v m_v^{3/2}|\mu_{cv}^z|^4)^2(\sum_v m_v^{3/2}|\mu_{cv}^z|^2)^{-2}I_1I_2 \tag{33b}$$

and

$$\sigma_0 = \alpha_0\ell \ . \tag{33c}$$

We used (11g) to obtain (33a). The parameter σ_0 may be called the optical thickness of the sample. If one wants to ignore the pump depletion, one can

let $\rho_o \to 0$ in (33a), which would then revert to the form that is obtained from (11b). Figure 4 shows (η/η_o) vs δ for various ρ_o. Above the band edge,

$$(\eta/\eta_o) \simeq 2\left[1-(4\delta^2)^{-1}\right]\exp\left(-\rho_o\sqrt{2|\delta|}\right). \tag{34a}$$

Thus, when the pump waves are undepleted, η has an upper limit which is $2\eta_o$ for frequency detunings that are large relative to the linewidth. For the specific semiconductor above and for $I_1 = I_2 = 1$ MW/cm^2 and $\tau = 10^{-11}$ sec, $2\eta_o \simeq .44 = 44\%$. Similarly, below the band edge,

$$(\eta/\eta_o) \simeq (2\delta^2)^{-1} \exp\left(-\rho_o/\sqrt{2\delta}\right), \tag{34b}$$

which decreases rapidly with increasing δ.

It is clear that the optimum place for phase conjugation is in the vicinity of the band edge. When the pump depletion is taken into account, there is more structure in the reflectivity as a function of the frequency detuning. Also, the reflectivity decreases as $\hbar\omega - E_G$ increases above the band edge. The reflectivity generally peaks in the vicinity of the band edge. The position of the peak is given by a fifth order equation which is obtained by setting the derivative of (η/η_o) with respect to δ equal to zero:

$$y^5 + y - (4/\rho_o) = 0 \tag{35a}$$

where

$$y \equiv \left(\sqrt{1+\delta^2} - \delta\right)^{1/2} . \tag{35b}$$

There is at least one root of Eq. (35a), say y_o, which is real and positive. The left-hand side can be expanded as

$$y^5 + y - (4/\rho_o) = (y-y_o)g(y) \quad , \tag{36a}$$

$$g(y) = y^4 + y_o y^3 + y_o^2 y^2 + y_o^3 y + y_o^4 + 1 \quad . \tag{36b}$$

The constant coefficients of g are all real and positive; therefore, the roots of g = 0 are all complex. This can be seen as follows. If there were another real root, it would have to be negative. Let y_1 be real and positive. For $y_1 > y_o$,

$$g(-y_1) = (y_1^3 + y_o^2 y_1)(y_1-y_o) + y_o^4 + 1 > 0 \quad . \tag{36c}$$

Similarly for $y_1 < y_o$,

$$g(-y_1) = (y_o^3 + y_o y_1^2)(y_o-y_1) + y_1^4 + 1 > 0. \tag{36d}$$

g is always positive for a real y and g=0 can have only complex roots. Thus, there is only one peak in the reflectivity. As ρ_o increases, the peak shifts to larger δ. It follows that if the semiconductor is saturated, the optimum place for phase conjugation is slightly above the band edge, and if there is significant absorption at ω, the place to be is slightly below the band edge.

ACKNOWLEDGEMENTS

We gratefully acknowledge the support of AFSOR for this work.

APPENDIX

For the convenience of the reader, we explicitly display the contour integrations which yield (7a) and (7b). After the angular integrations are performed, one obtains four types of integrals which can be written as

$$I_1(A) = \int_{-\infty}^{+\infty} dy\ y^2(y^2+A)^{-2}(y^2+A^*)^{-1} \quad , \tag{A-1}$$

$$I_2(A,B) = \int_{-\infty}^{+\infty} dy\ y^2(y^2+A)^{-1}(y^2+B)^{-1}(y^2+B^*)^{-1} \quad , \tag{A-2}$$

$$I_3(A) = \int_{-\infty}^{+\infty} dy\ y^2(y^2+A)^{-2} \quad , \tag{A-3}$$

$$I_4(A,B) = \int_{-\infty}^{+\infty} dy\ y^2\left[(y^2+A)^2 + B^2\right]^{-1} \tag{A-4}$$

The integrand of I_1 can be written as

$$y^2(y^2+A)^{-2}(y^2+A^*)^{-1} = A(A-A^*)^{-2}(y^2+A)^{-1} - A^*(A-A^*)^{-2}(y^2+A^*)^{-1} - (A-A^*)^{-1}y^2(y^2+A)^{-2} \quad . \tag{A-5}$$

An integration by parts gives

$$\int_{-\infty}^{+\infty} dy\ y^2(y^2+A)^{-2} = 2^{-1}\int_{-\infty}^{+\infty} dy(y^2+A)^{-1} \quad . \tag{A-6}$$

Thus,

$$I_1(A) = 2^{-1}(A-A^*)^{-2}\left[(A+A^*)\int_{-\infty}^{+\infty} dy(y^2+A)^{-1} - 2A^*\int_{-\infty}^{+\infty} dy(y^2+A^*)^{-1}\right] . \tag{A-7}$$

Let $A = a^2 e^{2i\phi}$, where a is real and positive and $-\frac{\pi}{2} \le \phi \le \frac{\pi}{2}$. There are two distinct roots for $y^2 + A = 0$, which are $y_0 = a \exp\left[i(\phi + \frac{\pi}{2})\right]$ and $y_1 = a \exp\left[i(\phi + \frac{3\pi}{2})\right]$. Closing the contour in the upper half,

$$\int_{-\infty}^{+\infty} dy\ (y^2+A)^{-1} = (\pi/a)\ \exp\ (-i\phi) \qquad (A\text{-}8)$$

$$= \pi(1+A^*/|A|)(2|A|+A+A^*)^{-1/2} .$$

Using (A-8) in (A-7), one finds that

$$I_1(A) = (\pi/4a^3)(1+\cos\ 2\phi)^{-1}\ \exp\ (-i\phi) \qquad (A\text{-}9)$$

$$= (\pi/2)(1+A^*/|A|)(2|A|+A+A^*)^{-3/2} .$$

The integrand of I_2 can be written as

$$y^2(y^2+A)^{-1}(y^2+B)^{-1}(y^2+B^*)^{-1} = -A(A-B)^{-1}(A-B^*)^{-1}(y^2+A)^{-1} \qquad (A\text{-}10)$$

$$-B(B-A)^{-1}(B-B^*)^{-1}(y^2+B)^{-1} - B^*(B^*-A)^{-1}(B^*-B)^{-1}(y^2+B^*)^{-1} .$$

Now use (A-8):

$$I_2(A,B) = -\pi\Big\{A(1+A^*/|A|)(A-B)^{-1}(A-B^*)^{-1}(2|A|+A+A^*)^{-1/2} \qquad (A\text{-}11)$$

$$+ B(1+B^*/|B|)(B-A)^{-1}(B-B^*)^{-1}(2|B|+B+B^*)^{-1/2}$$

$$+ B^*(1+B/|B|)(B^*-A)^{-1}(B^*-B)^{-1}(2|B|+B^*+B)^{-1/2}\Big\} .$$

$$= \pi(A-B)^{-1}(A-B^*)^{-1}\Big[(A+|B|)(2|B|+B+B^*)^{-1/2}$$

$$-(A+|A|)(2|A|+A+A^*)^{-1/2}\Big] .$$

In (A-3), an integration by parts yields

$$I_3(A) = 2^{-1}\int_{-\infty}^{+\infty} dy\ (y^2+A)^{-1} \qquad \text{(A-12)}$$

$$= (\pi/2)(1+A^*/|A|)(2|A|+A+A^*)^{-1/2}$$

Finally, the integrand of (A-4) can be written as

$$y^2\left[(y^2+A)^2+B^2\right]^{-1} = (i/2B)\left[(A-iB)(y^2+A-iB)^{-1} - (A+iB)(y^2+A+iB)^{-1}\right] , \qquad \text{(A-13)}$$

where A and B are real. Now using (A-8) yields

$$I_4(A,B) = (\pi/B\sqrt{2})(A^2+B^2)^{1/4}(\sqrt{A^2+B^2}\ -A)^{1/2} .$$

Let $z_o = (4\pi^2)^{-1}(2m_v/\hbar^2)^{3/2}$. Using (A-7), (A-11), (A-12) and (A-14), one finds

$$\int d\vec{k}(2\pi)^{-3}\ L_{vc}(\omega)|L_{vc}(\omega)|^2 = z_o I_1(\hbar\omega+E_G+i\gamma_{cv}) , \qquad \text{(A-15a)}$$

$$\int d\vec{k}(2\pi)^{-3}\ L_{cv}(\omega)|L_{cv}(\omega)|^2 = z_o I_1(E_G-\hbar\omega-i\gamma_{cv}) , \qquad \text{(A-15b)}$$

$$\int d\vec{k}(2\pi)^{-3}\ L_{vc}(\omega)|L_{cv}(\omega)|^2 = z_o I_2(E_G+\hbar\omega+i\gamma_{cv},E_G-\hbar\omega+i\gamma_{cv}) , \qquad \text{(A-15c)}$$

$$\int d\vec{k}(2\pi)^{-3}\ L_{cv}(\omega)|L_{vc}(\omega)|^2 = z_o I_2(E_G-\hbar\omega-i\gamma_{cv},E_G+\hbar\omega+i\gamma_{cv}) , \qquad \text{(A-15d)}$$

$$\int d\vec{k}(2\pi)^{-3}\left[L_{vc}(\omega)\right]^2 = z_o I_3(E_G+\hbar\omega+i\gamma_{cv}) , \qquad \text{(A-15e)}$$

$$\int d\vec{k}(2\pi)^{-3}\left[L_{cv}(\omega)\right]^2 = z_o I_3(E_G-\hbar\omega-i\gamma_{cv}) , \qquad \text{(A-15f)}$$

$$\int d\vec{k}(2\pi)^{-3}|L_{cv}(\omega)|^2 = z_o I_4(E_G-\hbar\omega,\gamma_{cv}) , \qquad \text{(A-15g)}$$

$$\int d\vec{k}(2\pi)^{-3}|L_{vc}(\omega)|^2 = z_o I_4(E_G+\hbar\omega,\gamma_{cv}) . \qquad \text{(A-15h)}$$

Collecting all of these together gives (7a) and (7b).

REFERENCES

1. R. K. Jain and M. B. Klein, Appl. Phys. Lett. 35(b) (1979) 454.

2. R. K. Jain, M. B. Klein and R. C. Lind, Opt. Lett. 4 (1979) 328.

3. R. K. Jain and D. G. Steel, Appl. Phys. Lett. 37(1) (1980) 1.

4. M. A. Khan, P. W. Kruse and J. F. Ready, Opt. Lett. 5 (1980) 261.

5. David Depatie and Donald Haueisen, Opt. Lett. 5 (1980) 252.

6. D. A. B. Miller, R. G. Harrison, A. M. Johnston, C. T. Seaton and S. D. Smith, Opt. Comm. 32 (1980) 478.

7. R. L. Abrams and R. C. Lind, Opt. Lett. 2 (1978) 94.

8. A. Elci, D. Rogovin, D. Depatie and D. Haueisen, J. Opt. Soc. Am. 70 (1980) 990.

9. See for example, D. Long, "Energy Band Structures of Mixed Crystals of III-V Compounds", in Semiconductors and Semimetals, Vol. I. Eds. R. K. Willardson and A. C. Beer (Academic Press, New York 1966).

10. P. A. Wolff and G. A. Pearson, Phys. Rev. Lett. 17 (1966) 1015.

11. In adapting Eq. (2-8) of Ref. 8 for the absorption coefficient, one should note that since the crystal orientation and the light polarization are fixed, it should be multiplied by 3. The factor (1/3) in the original formula comes from an angular average over atomic or molecular orientation.

12. For a specific example see A. Elci, et al., Phys. Rev. B16 (1977) 191.

13. E. O. Kane, "$\vec{k}\cdot\vec{p}$ Perturbation", in Semiconductors and Semimetals, Vol. 1, Eds. R. K. Willardson and A. C. Beer (Academic Press, New York 1966).

14. W. Heitler, Quantum Theory of Radiation (Oxford 1960); pg. 77. Note that the annihilation operator q_λ in this reference differs from b_λ by a normalization factor $(h/2\omega_\lambda)^{1/2}$.

15. T. S. Moss, G. J. Burrell and B. Ellis, Semiconductor Opto-electronics (Butterworth & Co., London 1973).

FIGURE CAPTIONS

FIGURE 1. Model band structure.

FIGURE 2. The geometry of four-wave mixing. A_3 and A_4 are the amplitudes of the conjugate and signal waves, respectively. A_1 and A_2 are the amplitudes of the pump waves.

FIGURE 3. $|\chi^{(3)}(\omega = \omega+\omega-\omega)|$ as a function of the frequency detuning per linewidth.

FIGURE 4. The reflectivity of conjugate waves as a function of the frequency detuning for various optical thicknesses.

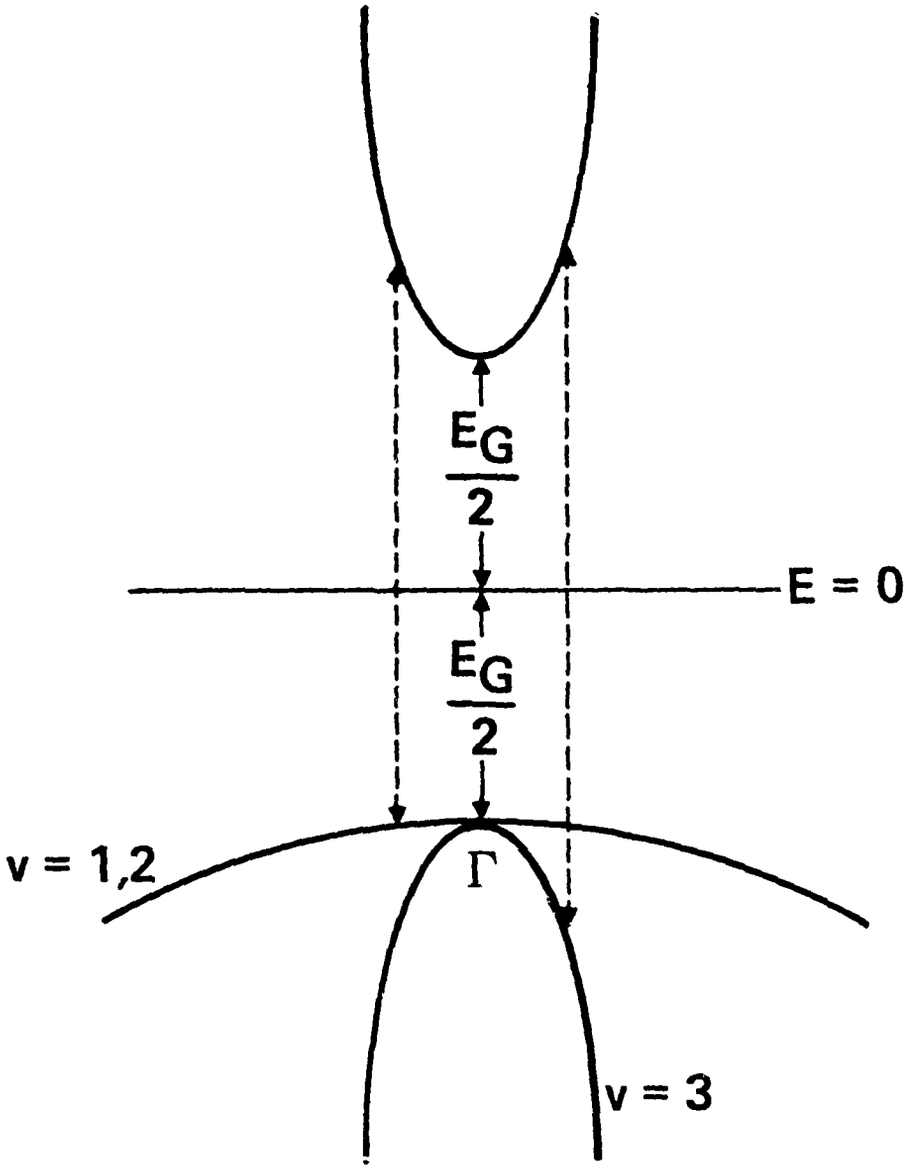

Figure 1

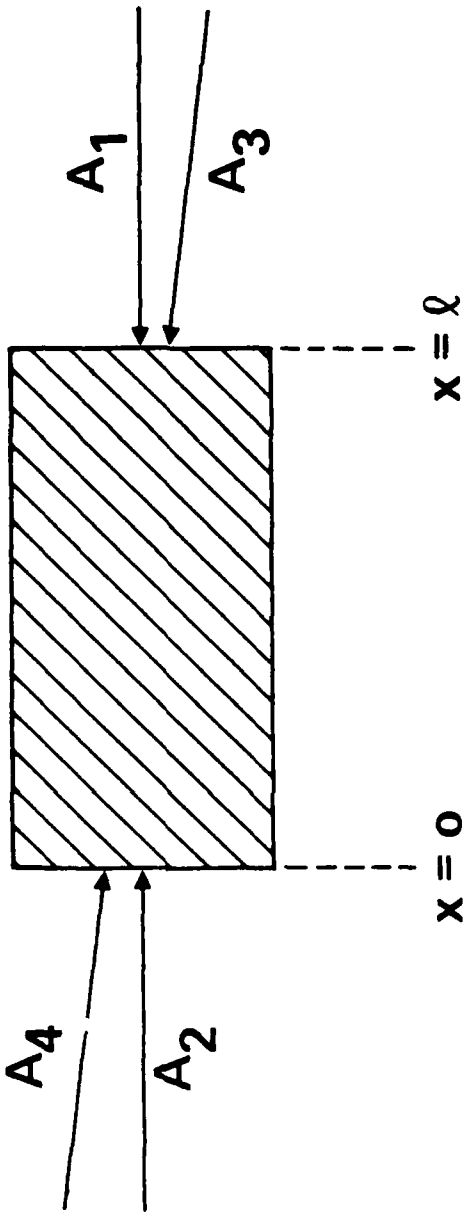

Figure 2

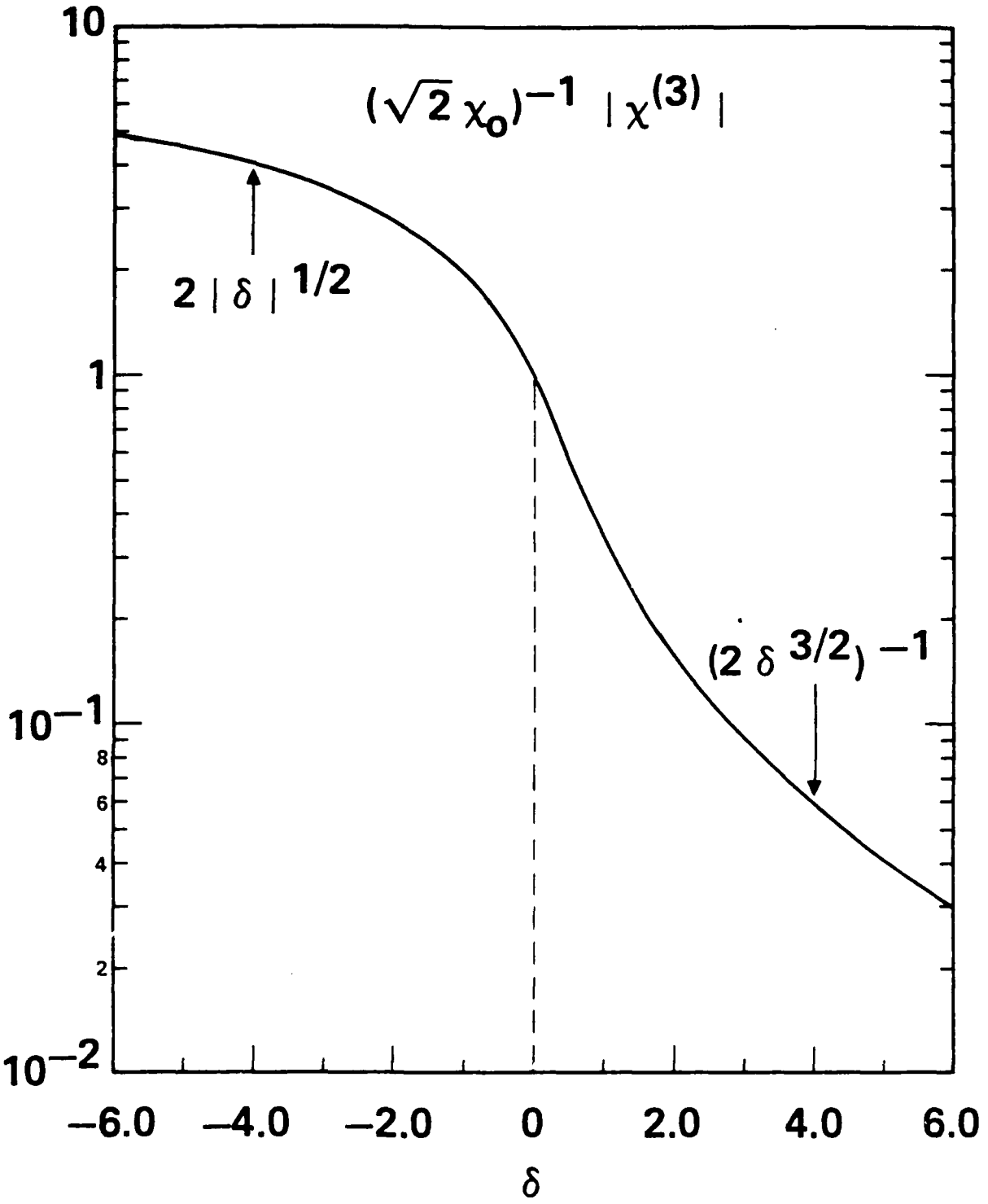
10
$(\sqrt{2}\,\chi_o)^{-1}\ |\chi^{(3)}|$
$2\,|\,\delta\,|^{1/2}$
1
10^{-1}
8
6
4
2
10^{-2}
$(2\,\delta^{3/2})^{-1}$
−6.0
−4.0
−2.0
0
2.0
4.0
6.0
δ

Figure 3

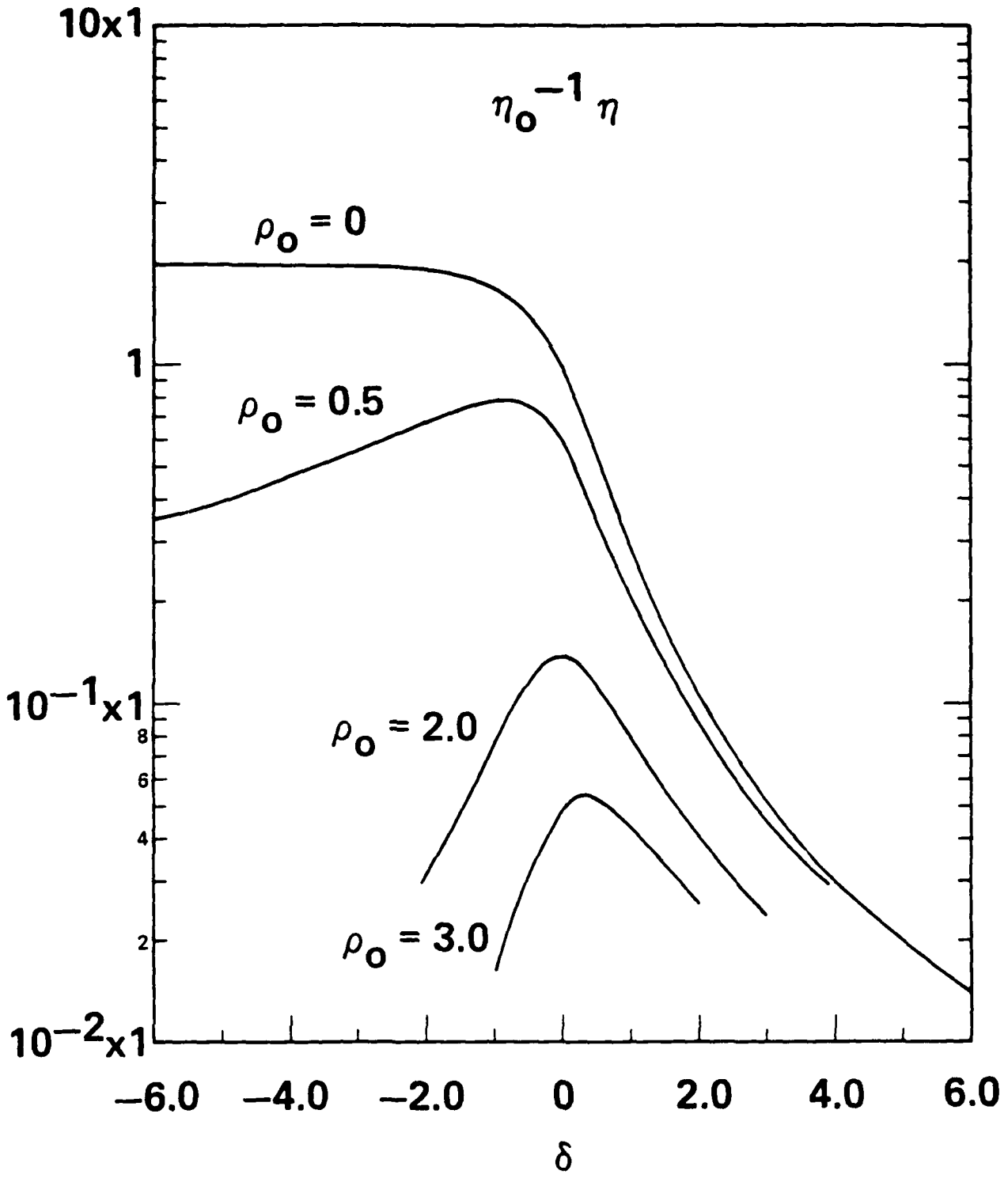
10x1
$\eta_o^{-1}\eta$
$\rho_o = 0$
1
$\rho_o = 0.5$
$10^{-1}x1$
8
6
4
$\rho_o = 2.0$
2
$\rho_o = 3.0$
$10^{-2}x1$
−6.0
−4.0
−2.0
0
2.0
4.0
6.0
δ

Figure 4

APPENDIX 3

THE USE OF EXAPNSIONS IN UNSTABLE RESONATOR MODES TO CHARACTERIZE NONLINEAR GAIN SYSTEMS

by

J. Nagel and D. Rogovin

THE USE OF EXPANSIONS IN UNSTABLE RESONATOR MODES TO CHARACTERIZE NONLINEAR GAIN SYSTEMS

by

J. Nagel and D. Rogovin
Science Applications, Inc.
1200 Prospect Street
La Jolla, California 92038

ABSTRACT: A series expansion in empty resonator modes is used to approximate the field in a cavity filled with a nonlinear gain medium. The time dependence of the expansion coefficients may be obtained using Maxwell's equations and orthogonality properties of the modes. The equations are solved numerically to determine the solutions in the vicinity of the stable point. The effects of changing the number of modes and the acuracy of the overlap integral are examined. The results are found to be most reliable for cavities where all modes but one are nearly suppressed and stable operation is possible. Self-sustaining pulsations between transverse modes and bistability were discovered for some conditions.

I. INTRODUCTION

In order to describe the time dependent properties of lasers it is natural to construct a set of first order equations of motion. The Maxwell equations for the laser fields are second order in both time and space derivatives and are therefore very difficult to work with directly. If one assumes that the fields may be represented by a time dependent expansion in free space modes, the spatial variations of the fields can be separated by inserting this expansion into the nonlinear Maxwell equations. Using orthogonality properties of the modes, and neglecting second order effects, there results a set of first order differential equations for the expansion coefficients of the laser field[1,2].

The free space modes are plane waves, which does not lead to much error for lasers with stable cavities or Fabry-Perot resonators. However, high energy systems often include unstable resonator cavities[3,4] because of their large mode volumes, excellent discrimination, and efficient output coupling. The modes of these cavities are quite different from plane waves, and may be obtained by solving the Fresnel-Kirchoff linear integral equation[5-8]. For such cavities expansions in empty resonator modes can be used to describe the spatial variations of the fields, and time dependent behavior may be treated in the usual way with a set of first order time differential equations for the expansion coefficients[9].

The careful treatment of the saturable gain problem for cw operated unstable resonators involves a nonlinear integral equation with a volume rather than a surface integral. In practice this approach proves to be intractible. Consequently, the equations of motion resulting from the use of expansions in unstable resonator modes should be useful for stable operation as well as for time dependent properties. In this paper the time dependent behavior in the vicinity of the stable point is examined.

In Section II the equations of motion for cylindrically symmetric homogeneously broadened lasers are developed with explicit expressions for the normalization and overlap integrals. The resulting equations of motion are in the form of Lamb Theory[1], and are in a sufficiently general form to include both transverse and longitudinal degrees of freedom. The numerical evaluation of the overlap integrals is outlined in Section III. Fast Hankel transforms were used to generate the unstable resonator modes in the interior of the cavity, and the volume integral was calculated with Simpson's rule. In Section IV, the stable solutions to the equations of motion are described, and the use of these solutions to calculate output couplings, frequency pulling effects, power fluctuations, and line broadening is discussed. The time dependent behavior in the vicinity of the stable point is treated by expressing the equations of motion in this region in the simpler Van der Pol form. In Section V, numerical results are given. An M = 2 cavity was used, with values of N_{eq} at both a peak and a crossing point of the $|\lambda|$ vs. N_{eq} curve. An examination of the accuracy of the overlap integrals and the necessary number of modes was made. It was found that for some situations the solutions of the equations of motion did not stabilize, and self-sustaining pulsations between transverse modes appeared, a phenomenon which cannot be explained by geometric optics descriptions. When one mode did achieve dominance, the energy distribution of the cavity was little affected by nonlinear gain, although the frequency pulling, output coupling, and linewidths were changed considerably from their empty resonator values. Finally, we conclude with a brief discussion of the use of expansions in unstable resonator modes to describe nonlinear systems.

II. EXPANSION IN EMPTY RESONATOR MODES

The empty resonator modes are eigenvalue solutions to the Fresnel-Kirchoff integral equation[10-12]. The kernel to this linear, homogeneous equation is non-hermitian and consequently the eigenvalue solutions do not form a complete set[13]. The solutions are orthogonal[14] and may be used to approximate an arbitrary function using a series expansion with overlap integrals to compute the expansion coefficients. The accuracy of this approximation is, in general, limited due to the non-completeness of the empty resonator modes. However, the specific function we wish to represent is the distribution of radiation on a cavity with a nonlinear gain medium and it is well known that this distribution is not very much different from the lowest loss empty resonator mode[15-18]. Therefore, one might expect an expansion in empty resonator modes to give reasonable results for the nonlinear problem. A relatively small number of terms in the series will be required, by contrast with a fourier series expansion of the transverse spatial dependence, which has a large number of terms due to the effects of edge diffraction. Since the difficulty of solution increases with n^3 where n is the number of terms in the series approximation, one is led to consider the use of empty resonator modes to describe nonlinear gain systems.

The electric field of an empty unstable resonator may be expressed as the following expansion in empty resonator modes:

$$E(\bar{r},t) = \sum_{n\ell q} b_{n\ell q}\, U_{n\ell q}(r,z) e^{i\ell\varphi} e^{i\omega_{n\ell q} t} \quad , \tag{1a}$$

$$U_{n\ell q}(r,z) = \left\{ a_F^{n\ell q}(r,z) e^{ik_{n\ell q}(L/2-z)} - a_B^{n\ell q} e^{-ik_{n\ell q}(L/2-z)} \right\} . \tag{1b}$$

In Eq. (1) a_F and a_B are forward and backward amplitudes, n labels the radial, ℓ the azimuthal and q the longitudinal degrees of freedom. The cavity is asssumed

to be cylindrical with equal mirrors. The amplitudes are related to the slowly varying mirror amplitude $\phi(x)$ by:

$$a_F^{n\ell q}(x,z) = (+i)^{\ell+1} 2\pi N \frac{L}{z} e^{-i\pi NLx^2/z} \int_0^1 ydy e^{-i\pi N(M^{-1}L-z)y^2/z}$$

$$X\ J_\ell(2\pi NLxy/z)\ \phi^{n\ell q}(y) \quad , \tag{2a}$$

$$a_B^{n\ell q}(x,z) = (-i)^{\ell+1}\ 2\pi N \frac{L}{z} e^{+i\pi NLx^2/z} \int_0^1 ydy e^{+i\pi N(M^{-1}z+L-z)y^2/z}$$

$$X\ J_\ell(2\pi NLxy/z)\ \phi^{n\ell q}(y). \tag{2b}$$

Here x and y are radial coordinates normalized to the mirror radius, M is the cavity magnification, N is the q dependent cavity Fresnel number, and $\phi^{n\ell q}(x)$ is the usual solution to the Fresnel-Kirchoff integral equation, a slowly varying function in the geometric optics limit. Both forward and backward amplitudes have been explicitly included because $a_F \neq a_B^*$ for lossy modes.

The $k_{n\ell q}$ and $\omega_{n\ell q}$ in Eq. (1) are complex quantities, determined by the eigenvalues of the Fresnel-Kirchoff integral equation. Each mode in Eq. (1) satisfies Maxwell's equations in the axial approximation with the mirror boundary conditions $E^i_{mirror} = 0$. Since $\omega_{n\ell q}$ has a positive imaginary part for all lossy modes, the radiation in the cavity decays with time. The complex part of $k_{n\ell q}$ compensates for the decrease in the magnitude of a_F as a wave propagates across the cavity in the forward direction. As a result Eq. (1) is symmetric under spatial inversion. If some radiation is introduced into the cavity, and enough time passes to form the mode patterns, the initial direction of the radiation launched into the cavity is forgotten. The radiation distribution is spatially symmetric about the midpoint of the cavity, and exponentially decreasing in time.

To account for time dependent properties in a more realistic manner, the expansion coefficients $b_{n\ell q}$ are assumed to be slowly varying functions of time. Since $b_{n\ell q}$ is complex, the $e^{i\omega_{n\ell q}t}$ term can be absorbed as follows:

$$b_{n\ell q}e^{i\omega_{n\ell q}t} \longrightarrow \gamma_{n\ell q}(t)e^{i\theta_{n\ell q}(t)} \quad , \tag{3}$$

where $\gamma_{n\ell q}$ and $\theta_{n\ell q}$ are real functions of t to be determined, and the instantaneous frequency of the mode is $\dot{\theta}_{n\ell q}$.

The resulting expansion is substituted into the wave equation for the cavity,

$$\left[\nabla^2 - \frac{1}{c^2}\frac{d^2}{dt^2}\right] E = \frac{1}{\varepsilon_o c^2}\frac{d^2}{dt^2} P(E) \quad , \tag{4}$$

where P is a complex function of the quasi-linear form P = g(E)E. On the left side, the usual axial approximation[19] is made which consists of neglecting second derivatives of $a_{F,B}$ with respect to z. Neglecting also second derivatives with respect to time, and taking into account that the amplitudes $a_{F,B}$ satisfy

$$\left(\nabla_\perp^2 \mp 2ik_{n\ell q}\frac{d}{dz}\right)a_{F,B} = 0 \quad , \tag{5}$$

the left side of Eq. (4) is:

$$\left\{(\dot{\theta}^2_{n\ell q} - k^2_{n\ell q}c^2)\,\gamma_{n\ell q} - 2i\,\dot{\theta}_{n\ell q}\,\dot{\gamma}_{n\ell q}\right\}U_{n\ell q}(r,z)e^{i\ell\psi} \quad , \tag{6}$$

where $U_{n\ell q}(r,z)$ is the spatial part of the mode, given by Eq. (1b).

Next, two further approximations are made which are consistent with the neglect of second order effects:

$$\dot{\theta}^2_{n\ell q} - k^2_{n\ell q} c^2 \sim 2\omega (\dot{\theta}_{n\ell q} - k_{n\ell q} c) \quad , \tag{7a}$$

$$\dot{\theta}_{n\ell q} \dot{\gamma}_{n\ell q} \sim \omega \dot{\gamma}_{n\ell q} \quad . \tag{7b}$$

Here ω is a real frequency equal to $\pi qc/L$, where q is the longitudinal mode number.

The right side of Eq. (4) is a complicated nonlinear function, and for many cases the linear gain is large. For behavior near the stable point, saturation is a factor, and $\dot{\gamma} \sim g(E)c$. Then the right side of Eq. (4) is small to first order, and may be replaced by

$$-\frac{\omega^2}{\varepsilon_o c^2} \; g(E)E. \tag{8}$$

Next, multiply both sides of the resulting equation by

$$a_B{}^{n'\ell'q'} \; e^{-i\ell'\psi'} \; e^{ik_{n'\ell'q'}(z-L/2)} \; e^{-i\theta_{n'\ell'q'}} \tag{9}$$

and integrate over all χ,r,z, taking into account the orthogonality properties of the empty resonator modes. Define the normalization matrix W and the polarization matrix P by:

$$W_{n'\ell'q',\, n\ell q} = \langle a_B{}^{n'\ell'q'} \; e^{ik_{n'\ell'q'}(z-L/2)} \; U^{n\ell q} \; e^{i(\ell-\ell')\psi} \rangle_v \; , \tag{10a}$$

$$P_{n'\ell'q',n\ell q} = \langle a_B{}^{n'\ell'q'} e^{ik_{n'\ell'q'}(z-L/2)} \; g(E) U^{n\ell q} \; e^{i(\ell-\ell')\psi} \rangle_v, \tag{10b}$$

where $< >_v$ represents an average over the cavity volume. The matrices W and P are diagonal in ℓ for most reasonable functions g(E).

The complex form for $k_{n\ell q}c$ is

$$k_{n\ell q}c = \omega + \beta_{n\ell q} + i\Gamma_{n\ell q}c \quad , \tag{11}$$

where $\beta_{n\ell q}$ is a diffractive frequency shift, $\Gamma_{n\ell q}$ the diffractive loss, and both β and Γc are $<< \omega$. Finally, the cavity equations reduce to the following simple rate equations:

$$\dot{\gamma}_{n\ell q} + c\Gamma_{n\ell q}\,\gamma_{n\ell q} = \frac{\omega}{2\varepsilon_o}\,\mathrm{Im}\,(W^{-1}P\gamma)_{n\ell q} \quad , \tag{12a}$$

$$\gamma_{n\ell q}\,(\dot{\theta}_{n\ell q} - \beta_{n\ell q} - \omega) = \frac{-\omega}{2\varepsilon_o}\,\mathrm{Re}(W^{-1}P\gamma)_{n\ell q} \quad . \tag{12b}$$

Explicit forms for the normalization matrix W and the polarization matrix P are given below. The orthogonality relation between transverse modes of the same longitudinal wave is given by:

$$\langle a_B^{n'\ell'q}\, a_F^{n\ell q}\, e^{i(k_{n'\ell'q} - k_{n\ell q})(z-L/2)}\, e^{i(\ell-\ell')\psi} \rangle_v =$$

$$\delta_{nn'}\delta_{\ell\ell'} \int_0^1 y\,dy\, e^{-i\pi N(M-M^{-1})y^2}\, \phi^{n'\ell'q}(y)\phi^{n\ell q}(y) \quad , \tag{13}$$

where $\phi^{n\ell q}$ is the Fresnel-Kirchoff solution.

The rapidly oscillating quadratic term in the integrand results from the opposite curvatures of the forward and backward waves. In order to evaluate the interior amplitudes a_F and a_B using the Fresnel-Kirchoff solutions, it proves convenient to define the following auxilliary functions in Hankel transform space:

$$\phi_F^{n\ell q}(Q) = H\left[e^{-i\pi N(M-1)y^2}\,\phi^{n\ell q}\right], \tag{14a}$$

$$\phi_B^{n\ell q}(Q) = H\left[e^{i\pi N(M^{-1}-1)y^2}\,\phi^{n\ell q}\right], \tag{14b}$$

where $\phi^{n\ell q} = 0$ outside the mirror, for $x > 1$. The Hankel transformed interior amplitudes are given by Eq. (22). The integral in Eq. (13) in terms of these auxilliary functions is:

$$\delta_{nn'}\,\delta_{\ell\ell'}\int_0^\infty QdQ\;\phi_B^{n'\ell'q}(Q)\;\phi_F^{n\ell q}(Q) \quad . \tag{15}$$

Using Eqs. (2), (10), (14), and (15), it is easy to derive the following form for the W matrix:

$$W_{n'\ell'q',\,n\ell q} = \delta_{\ell\ell'}\left\{S_{n'\ell'q',\,n\ell q} - T_{n'\ell'q',\,n\ell q}\right\}, \tag{16}$$

where

$$S_{n'\ell'q',\, n\ell q} = \frac{1}{L} \int_0^L dz e^{i(k_{n'\ell'q} - k_{n\ell q})(z-L/2)}$$

$$\times \int_0^\infty Q dQ e^{-i\pi(N-N')zQ^2/LNN'} \phi_B^{n'\ell'q'}(Q)\, \phi_F^{n\ell q}(Q), \qquad (17a)$$

$$T_{n'\ell'q',\, n\ell q} = \frac{1}{L} \int_0^L dz e^{i(k_{n'\ell'q} + k_{n\ell q})(z-L/2)}$$

$$\times \int_0^\infty Q dQ e^{-i\pi(N+N')zQ^2/LNN'} \phi_B^{n'\ell'q'}(Q) \phi_F^{n\ell q}(0) \; . \qquad (17b)$$

For large q, it is an extremely good approximation to set T = 0 because of the rapidly oscillating z dependence of the integrand. When this is done, the theory is identical to that of reference (9). Note that for q' = q, N' = N and Eq. (17a) reduces to Eq. (15) due to the orthogonality properties of the empty resonator modes.

The evaluation of the P matrices depends on the specific form for the nonlinear susceptibility. In general, the calculation involves complicated overlap integrals. The homogeneous broadening form for the nonlinear susceptibility is used here,

$$g(E) = i g_0 \varepsilon_0 c/\omega \, (1+|E|^2)^{-1} \quad , \qquad (18)$$

where $|E|^2$ has been normalized to the saturation intensity, and g_0 is the linear gain. Couplings between modes of different ℓ are neglected, as well as couplings

between different longitudinal modes. Interference between forward and backward waves is expected to be significant for unstable cavities[20]. The frequency dependence for g(E) is not specified, since the laser linewidth is assumed to be set by the cavity and not the medium.

As in Eq. (16) for W, the integral for P splits into two terms. However the term analogous to T in Eq. (17b) is no longer negligible because nonlinear coupling between forward and backward waves leads to a slowly varying component of the z-integral and hence a non-zero contribution to the integral. After some calculation, the effective P matrix is found to be

$$P_{n'\ell'q',\, n\ell q} = \delta_{\ell\ell'}\delta_{qq'}\, ig_o\, \varepsilon_o\, c/\omega L \int_o^L dz e^{(\Gamma_{n'\ell'q'}-\Gamma_{n\ell q})(z-L/2)}$$

$$\times \int_o^1 y dy a_B^{n'\ell'q'}(y,z)\, f^{n\ell q}(y,z) \quad . \tag{19}$$

Here the Γ's are the losses as in Eq. (11), and f is given by:

$$f^i(y,z) = \frac{a^i_F(y,z)}{\sqrt{A^2-B^2}} \left(1 - \frac{A - \sqrt{A^2-B^2}}{2\left|\sum_i \gamma_i e^{i\theta_i} \Gamma_i (z-L/2) a_F^i\right|^2}\right) , \tag{20}$$

where

$$A = 1 + \sum_{i,j} \gamma_i\gamma_j e^{i(\theta_i-\theta_j)} \left(a_F^i a_F^{*j} e^{(\Gamma_i+\Gamma_j)(z-L/2)}\right.$$

$$\left. + a_B^i a_B^{*j} e^{-(\Gamma_i+\Gamma_j)(z-L/2)}\right) , \tag{21a}$$

$$B = 2\left|\sum_{i,j} \gamma_i\gamma_j e^{-i(\theta_i-\theta_j)} e^{(\Gamma_i-\Gamma_j)(z-L/2)} a_F^{*i} a_B^j\right| . \tag{21b}$$

Here the indices i,j are shorthand for the mode indices nℓq. Setting B = 0 in Eq. (20) is equivalent to neglecting the effects of interference between forward and backward waves.

III. EVALUATION OF OVERLAP INTEGRAL

The solutions to the Fresnel-Kirchoff integral equation may be obtained by well known methods[5-8]. The empty resonator modes and eigenvalues used here were calculated using the Butts-Avizonis asymptotic method, with the following general form[8] substituted for their F(x,t) function:

$$F(x,t) = K_1[1] = -i^{\ell} e^{-it(1+x^2)} \sum_{k=0}^{\infty} (ix)^k J_k(2tx) \quad , \tag{22}$$

where $t = \pi NM$, and $K[\cdot]$ is the Fresnel-Kirchoff integral transform. The mirror amplitude ϕ is given in terms of the basis functions by

$$\phi(x) = 1 + \sum_{n=1}^{N} a_n F_n(x) \quad . \tag{23}$$

Here a_n is obtained by finding the roots of a N^{th} - order polynomial and

$$F_n(x) = F(x/M^{2n}, t/M_{n-1}) \quad , \tag{24}$$

where $M_n = \sum_{k=0}^{n} M^{-2k}$. The eigenvalues and eigenvectors for the six lowest loss modes for both the Neq = 6.5 and Neq = 7.02 M = 2 resonator were obtained and stored on disc and used as data for the mode mixing calculation. Only the $\ell = 0$ case was treated. The losses and shifts for these modes are obtainable from the eigenvalues and are given in Table I.

Next the auxilliary functions $\phi_F{}^{n\ell q}(Q)$, $\phi_B{}^{n\ell q}(Q)$ in Q-space defined by Eq. (15) are calculated using the Fast Hankel Transform (FHT) algorithm[21], which approximates the Hankel transform by a finite transform. Since the interior values of the amplitudes are determined from the Fresnel-Kirchoff solution by the application of a finite Hankel transform, the FHT is particularly

Table I. Losses in percent and frequency shifts in units of c/2L for the six lowest loss modes of the N_{eq} = 6.50 and N_{eq} = 7.02 M = 2 empty resonators.

	L_1	L_2	L_3	L_4	L_5	L_6	$\Delta\omega_1$	$\Delta\omega_2$	$\Delta\omega_3$	$\Delta\omega_4$	$\Delta\omega_5$	$\Delta\omega_6$
$N_{\ell q}$=6.50	60.70	70.19	73.96	82.84	82.86	87.30	0.037	1.615	-1.655	3.956	-3.716	5.939
$N_{\ell q}$=7.02	64.00	64.00	77.78	80.03	80.93	85.13	-0.670	0.613	2.547	-2.604	-5.138	4.881

appropriate for this application. The conditions for the accuracy of the FHT are well known[21], and lead to the following mesh for x and Q space:

$$
\begin{aligned}
x_n &= x_o e^{\alpha n} \\
Q_n &= Q_o e^{\alpha n} \\
\alpha &= 1/4\beta \\
x_o &= e^{-\alpha M} \\
Q_o &= \beta x_o \quad ,
\end{aligned}
\tag{25}
$$

where β is the highest spatial frequency component considered, chosen here to be 2.5 $N_{FRESNEL}$, the lowest truncation point is less than 1/4 of the highest spatial frequency, and M = 512 is the number of points in the mesh.

Once $\phi_F(Q)$ and $\phi_B(Q)$ are known, the Hankel transformed interior amplitudes are simply:

$$
a_{F,B}(Q,z) = e^{\pm i\pi Q^2 z/NL}\, \phi_{F,B}(Q) \quad . \tag{26}
$$

The transverse spatial dependence of the interior amplitudes is found by again Hankel transforming Eq. (26). For each interior point z, the amplitude is given as an M-vector. Finally f(x,z) is determined from Eq. (20) and the double integral in Eq. (19) is evaluated using the trapezoidal rule. It is only necessary to integrate halfway across the cavity due to the symmetry of the problem.

The number of points in the z axis grid does not have to be very large. Numerical solutions of the nonlinear integral equation assume that the nonlinear gain is concentrated on a small number of thin slabs, and free space propagation

is used in the intervals between the slabs. Free space propagation is given by Eq. (26), and it may easily be seen that the use of the trapezoidal rule with n_{slab} points in the z grid is just as accurate as the evaluation of the nonlinear Fresnel-Kirchoff integral transform using the same number of thin slabs. The single thin slab approximation has been used extensively for low loss cavities[15-17], and has gives reasonable results in this regime. Consequently, a relatively small number of gain slabs should be sufficient to describe the radiation in more lossy cavities. For the present calculation we used $5 < n_{slab} < 45$, and making the grid finer did not change the results significantly, (see Figure 5).

IV. SOLUTIONS

CW laser operation may be adequately described by the stable solution to the equations of motion. The time dependence of the fields in the immediate vicinity of the stable point specifies such quantities as the frequency fluctuation, power fluctuation, and the field spectrum. Consequently, we first consider the stable solutions to Eq. (12).

The determination of the stable point involves solving a set of coupled, nonlinear equations. This was done in the present case by setting $\dot{\gamma}_i = 0$, rewriting the equations in the form $x = f(x)$, then using iteration, $x_{j+1} = f(x_j)$. This nonlinear mapping can lead to limit cycles or chaotic behvior rather than a stable point in some cases[22]. The stable solutions to the resulting n complex equations give the n γ_i's, the n-1 relative phases $\theta_i - \theta_{i-1}$, and the transverse frequency shift $\Delta\omega$, for a total of 2n real variables. Only the relative phases may be determined because the nonlinear term contains E in the form $|E|^2$, which is invariant to overall phase translations. The frequency shift $\Delta\omega$ is the locked value of the transverse frequencies, and is related to the phases by $\dot{\theta}_i - \omega = \Delta\omega$.

It may seem surprising that the frequencies should lock together, since the transverse frequencies are often spaced further apart than the longitudinal frequency separation c/2L, and the susceptibility is purely imaginary, at each point in space. However, an effective nonlinear index of refraction arises from the coupling of edge diffracted rays in the center of the cavity. Due to the complicated phase dependence of the individual modes, the overlap integrals in Eq. (12) are not purely imaginary, even though the susceptibility is. The overlap integral coupling between modes is non-local in nature, and this type of coupling can lead to frequency-pulling effects even if the index of refraction is locally linear. Since changing the relative phases changes $|E|^2$ and therefore affects the overlap integrals, transverse mode locking can occur.

This type of mode locking is different from the case where longitudinal mode frequency differences lock together leading to the formation of pulses[2]. For unstable cavities, the transverse frequencies are spread so irregularly that it is difficult for population pulsations at the frequency differences to appear. If there is coupling between a number of different longitudinal modes, a case can be envisioned where all the transverse modes of each longitudinal mode lock together, and the differences between longitudinal frequencies then lock together by the usual means.

Once the stable solution for γ_i and θ_i is obtained, the mirror amplitude is given by $\phi(x) = \Sigma_i \gamma_i e^{i\theta_i} \phi_i(x)$ and the locked frequency of the transverse modes by $\omega + \Delta\omega$. The output coupling for the stable solution may be determined from the effective eigenvalue, defined by

$$\lambda_{eff} = \frac{\langle \phi K \phi \rangle}{\langle \phi \phi \rangle} \quad , \tag{27}$$

where ϕ is the converged mirror amplitude, the brackets represent a mirror average, and K is the linear Fresnel-Kirchoff integral transform which propagates the solution once across the empty cavity. Using the expansion of ϕ in empty resonator modes and orthogonality properties, one finds

$$\lambda_{eff} = \frac{\Sigma_i \lambda_i \gamma_i^2 e^{2i\theta_i} \langle \phi_i^2 \rangle}{\Sigma_i \gamma_i^2 e^{2i\theta_i} \langle \phi_i^2 \rangle} \quad , \tag{28}$$

where λ_i are the eigenvalues of the empty resonator modes. The losses are given by $1 - |\lambda_{eff}|^2$.

To study the fluctuations about the stable point, a set of Langevin equations may be formed by adding random noise terms on the right side of Eq. (12). Alternatively, Eq. (12) may be used to write down the Fokker-Plank equation for the system[23]. Due to the complicated nature of the right hand

side of Eq. (12), neither of these approaches is useful unless one is able to solve the resulting equations numerically.

Here we take another approach which is approximate, yet provides qualitative insight into the behavior of the system as well as yielding useful numerical predictions. The equations of motion, Eq. (12), in the vicinity of the stable point are approximated by a simpler form which may be treated analytically, that of a Van der Pol oscillator[2]:

$$\dot{\gamma}_i = \alpha_i \gamma_i - \sum_j \beta_{ij} \gamma_i \gamma_j^2 \tag{29a}$$

$$\dot{\theta}_i - \omega = \sigma_i - \sum_j \rho_{ij} \gamma_j^2 \quad . \tag{29b}$$

Here and are symmetric, and the relative phases are assumed to be fixed. The α_i, σ_i, β_{ij}, and ρ_{ij} parameters were chosen by numerically evaluating $\dot{\gamma}_i$ and $\dot{\theta}_i$ using Eq. (12) for a large number of randomly chosen γ_i in the immediate vicinity of the stable point, and then least squares fitting to the form Eq. (29) with the restrictions that $\dot{\gamma}_i = 0$ and $\dot{\theta}_i = \omega + \Delta\omega$ at the stable point.

The Fokker-Plank method is used here, and the noise terms added on the right hand side of Eq. (29) are assumed to be Markovian:

$$\langle n_\gamma(t)\, n_\gamma(t') \rangle = D\, \delta(t-t') \tag{30a}$$

$$\langle n_\theta(t)\, n_\theta(t') \rangle = R\, \delta(t-t') \quad . \tag{30b}$$

This assumption leads to flat spectra for the power fluctuations, frequency fluctuations, and field. To obtain more realistic predictions for the spectral behavior or these quantities, a Langevin equation treatment should be used.

The next approximation is to consider only the amplitude noise term, Eq. (30a). By neglecting phase fluctuations, the Fokker-Plank equation can be solved trivially since Eq. (29a) may be derived from a potential. Amplitude fluctuations will lead to frequency shifts through Eq. (29b), which is assumed to react instantaneously to small amplitude fluctuations.

With these assumptions, the solution to the Fokker-Plank equation is

$$P(\gamma_1 \ldots \gamma_n) = N^{-1} \exp\left\{(2\alpha\gamma^2 - \gamma^2\beta\gamma^2)/2D\right\}, \tag{31}$$

where γ^2 is the vector γ_i^2, is the vector α_i, β is the matrix β_{ij}, and N is a normalization constant. Eq. (31) can be used to obtain estimates for the power fluctuations by assuming that all of the amplitudes except the largest is fixed at its stable value, and finding the point where P drops 1/2 of its value at the stable point. The FWHM of the power fluctuations is approximately:

$$\Delta I/I \sim 2\Delta\gamma_1/\gamma_1 \sim \sqrt{\frac{8D\ln 2}{\gamma_1^4 \beta_{11}}}, \tag{32}$$

where γ_1 is the largest mode amplitude.

To obtain a rough estimate for the frequency broadening due to amplitude fluctuations, only those fluctuations which maintain the frequency locking of the modes are assumed to be relevent. The locked frequency itself is buffeted about by these fluctuations. This assumption enormously simplifies the calculations and is expected to give reasonable results for the frequency broadening. In fact, results for the field spectrum $E(\omega)$ obtained using this method agreed well with a more exact calculation made for the cases of 1, 2, and 3 modes. Requiring $\dot{\theta}_i - \omega$ to be a single constant determines a point in γ^2 space through Eq. (29b), and the multidimenional distribution P in Eq. (31) is then reduced to a one-dimensional dependence on $\dot{\theta}_i - \omega = \delta\omega$:

$$P(\delta\omega) = N^{-1} \exp\left\{(-2\alpha\rho^{-1}\mu - \mu\rho^{-1}\beta\rho^{-1}\mu)/2D\right\}. \tag{33}$$

Here ρ and β are the matrices ρ_{ij} and β_{ij}, α is the vector α_i, and μ is the vector $\dot{\theta}_i - \omega - \sigma_i = \delta\omega - \sigma_i$. The broadening is obtained by determining the full width at half maximum of $P(\delta\omega)$, and is easily seen to be:

$$\Delta\omega = \sqrt{\frac{8D\ln 2}{\sum_{i,j} (\rho^{-1}\beta\rho^{-1})_{ij}}} \quad . \tag{34}$$

It is necessary to give some value for D in order to obtain numerical results. The noise term arises from spontaneous emissions, so one expects D to be small for large coherent intensities and large if the lifetime of the upper laser state is small. Also, D should be directly proportional to the number of atoms in the upper laser state. To determine D, one calculates the total energy stored in a Van der Pol oscillator driven by a random noise term, $n\gamma(t)$[24]. The total energy is obtained in terms of the power spectrum of $n_\gamma(t)$, $W_{n\gamma}(\omega)$. When this energy is set equal to the energy in the cavity due to spontaneous emission, $W_{n\gamma}$ is determined and D is then obtained from

$$D = \pi W_{n\gamma}(\omega_\ell) \quad , \tag{35}$$

where ω_ℓ is the laser frequency. The result, taking into account the particular definitions of the γ_i's and the fact that Eq. (29) was obtained from a calculation which used the dimensionless time $x = ct/2L$, is:

$$D = \frac{\hbar^2 \omega_\ell{}^3 N_2}{4\pi^2 t_2 L N I_s{}^2} \quad . \tag{36}$$

Here D is dimensionless, as are α, β, and x, N_2 is the number density of the upper laser state, t_2 is the lifetime of the upper laser state, L is the cavity length, N the cavity Fresnel number, and I_s is the saturation intensity. With the above relation for D, the power fluctuation and frequency broadening may be estimated.

V. RESULTS

The main purpose of the calculations was to examine the usefulness of the idea of expressing the field of a loaded unstable resonator as a superposition of empty resonator modes. In all cases, coupling between transverse modes only was considered. Since only one longitudinal mode was present, this corresponds to what is usually referred to as single mode operation. By gradually increasing the number of transverse modes until the resulting spatial distributions and frequencies of the stable solutions converged, it was found that a relatively small number of modes were needed for an accurate description. In addition both the transverse and the longitudinal accuracy of the overlap integral was varied, with grid density increasing until the results converged. Finally, an examination of the behavior in the vicinity of the stable point was examined by using fits to Eq. (29). From these, the power and frequency fluctuations were estimated.

Two separate sets of calculations were made for cavities with M = 2, with Neq = 6.5 or 7.02. On the plot of eigenvalues versus equivalent Fresnel number Neq for an M = 2 resonator, there is a peak at Neq = 6.5 and a minimum at Neq = 7.02. At the peaks, which occur near half integral values of Neq, the lowest loss mode is well separated from the other modes. By contrast, the minimums occur near integral values of Neq and result from the crossing of two separate empty resonator modes having the same loss. The two sets of conditions should pretty well characterize the response of an M = 2 cavity to a nonlinear gain medium. The magnitudes and phases of the eigenvalues for the Neq = 6.5 and Neq = 7.02 empty resonator modes are given in Table I.

First, the dependence of the stable solution on gain was examined. The results for the Neq = 6.5 three mode cavity, with a very coarse integration mesh $n_{slab} = 5$ are shown on Figure 1 in the form of a plot of the area-averaged mirror intensity vs. gain. Three modes were included because the second and third states have equal losses and thus should be considered together. As expected, the lowest loss mode has the largest coefficient, although as gain increases the coefficients of the lossy modes become somewhat larger. Also shown

on Figure 1 are the geometric optics area-averaged mirror intensities obtained by solving the Rigrod equations for the cavity, with couplings between forward and backward waves included[13,25]. Note that the threshold for the geometric optics case occurs at $g_0L = 1.39$, corresponding to the geometric optics eigenvalue $|\lambda| = M^{-1} = .5$. The threshold for the three-mode solution with full transverse field variation occured at the lower value $g_0L = .93$, corresponding to the eigenvalue of the lowest loss mode $|\lambda| = .627$. All three modes are less lossy than the geometric optics predictions because diffraction couples radiation from the edges back into the center of the cavity.

The geometric optics calculation results in a larger average intensity than is found in the more careful three-mode treatment. One reason for this is that as gain increases, the lossy modes become excited and therefore output coupling increases. On the other hand, output coupling remains independent of gain for geometric optics, and therefore one expects larger fields in this case. Also, the area averaging weights the edge region disproportionately, where the geometric optics wave is markedly larger than the lossy modes. In any case, the geometric optics results give qualitatively reasonable predictions, as long as there actually is a stable solution to the problem.

As gain is increased further, oscillations eventually appear in the three-mode solution and the iteration does not converge, even though the geometric optics problem has stable solutions for arbitrary gain. This behavior is much more obvious for the Neq = 7.02 cavity, where there are two modes of equal loss competing for gain. For this cavity a large number of calculations were made for the two mode problem with $n_{slab} = 10$ at different levels of gain. Since these two modes have equal losses, the problem cannot be further simplified. To check that two modes were enough, calculations were done for various gains with 3, 4, and 6 modes, and the results were found to be qualitatively the same as for the two mode problem, because all the higher order modes had small coefficients.

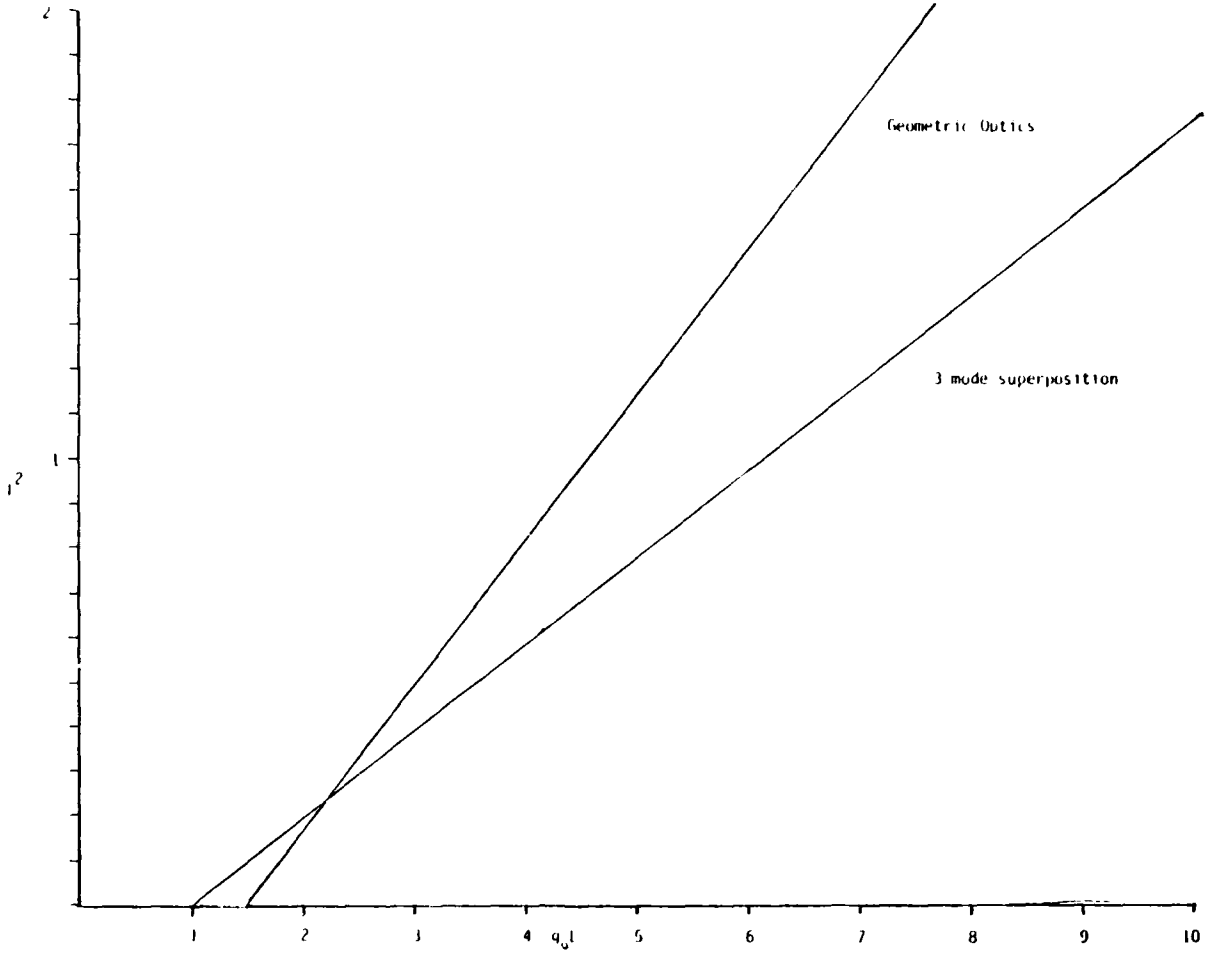

Figure 1. The mirror averaged intensition versus linear gain for the N_{eq} = 6.5 cavity. The three transverse mode solution is compared with the geometric optics predictions, which are given by the upper line.

At least one stable solution was found for each linear gain. The converged values of γ_1 and γ_2 for $g_0L < 8$ are given in Figure 2. Near threshold, γ_1 is largest. As gain is increased, γ_2 increases continuously, and near $g_0L = 6$ γ_2 suddenly becomes the dominant mode. Above this point, and at least until $g_0L = 150$, γ_1 is nearly suppressed. In the region $5.7 < g_0L < 6$ two separate stable solutions were found, implying the existence of bistable operation for this cavity. It is interesting to note that for unstable cavities, a locally nonlinear index of refraction[26] is not needed in order for bistability to occur. The discontinuity in the solutions near $g_0L = 6$ was not found for the $N_{eq} = 6.5$ cavity and is typical of bistable systems. The discontinuity is also evident in the mirror averaged intensities as gain is increased or decreased through the bistable regime. It is expected that there is a regime of stationary solutions which joins the two branches of stable solutions, but are unstable to small perturbations. Our algorithm was not designed to obtain these types of solutions.

In addition to stable solutions, self-sustaining pulsations were discovered in the region of bistability. For some initial conditions, the interative procedure did not converge to a stable point but to a limit cycle. Limit cycles for $g_0L = 6$ and $g_0L = 7$ are displayed in Figures 3 and 4. Similar limit cycles were also found for the four mode problem, so the phenomenon is not a result of the two mode restriction. The existence of a limit cycle implies that periodic self-sustaining pulsations between the two lowest loss modes occurs as the solution traverses the limit cycle. It is interesting that either a stable solution or pulsating behavior can occur for the same cavity at a specific gain, depending on the initial conditions.

As gain is increased, the effective coupling between modes increases. For small gains, both modes can oscillate at the same time, but as coupling is increased, a point is reached where one mode is suddenly suppressed. This evidently occurs near $g_0L = 6$. For larger gains, the solution with both modes oscillating is not stable and this is precisely where we find the limit cycles representing periodic pulsations between the two modes. Both modes are trying to oscillate at once, and the strong coupling leads to instability.

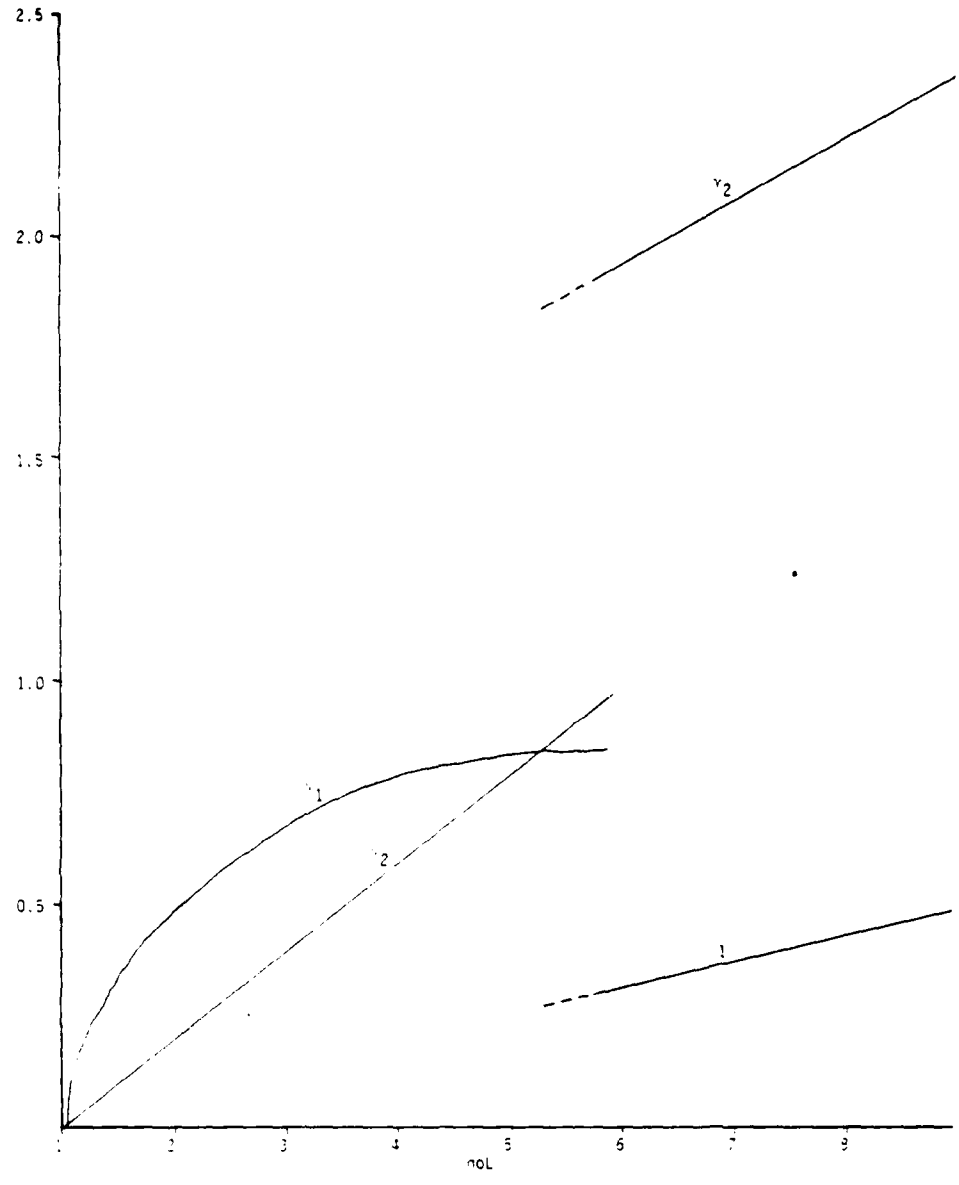

Figure 2. The stable solutions for the amplitudes of the lowest loss modes of the N_{eq} = 7.02 cavity for $g_0L < 8$. Two stable solutions were found in the region near $g_0L = 6$.

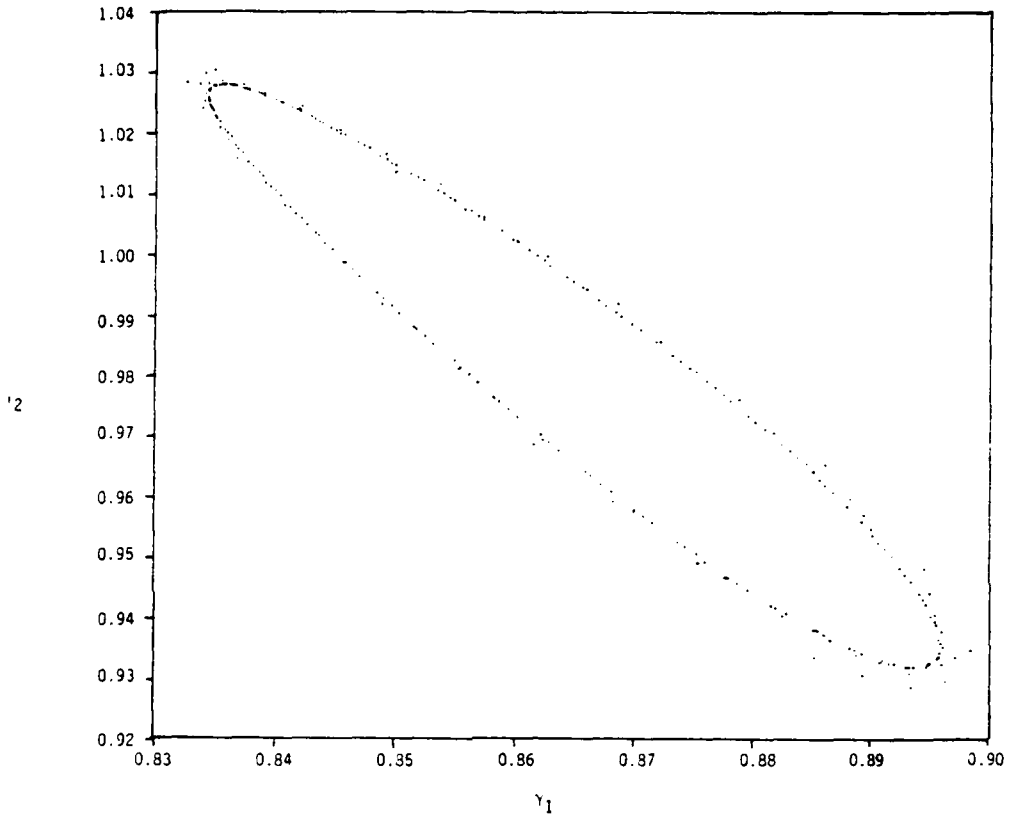

Figure 3. A limit cycle repr.. nting self-sustaining pulsations for the two mode N_{eq} = 7.02 cavity at $g_o L$ = 6.0.

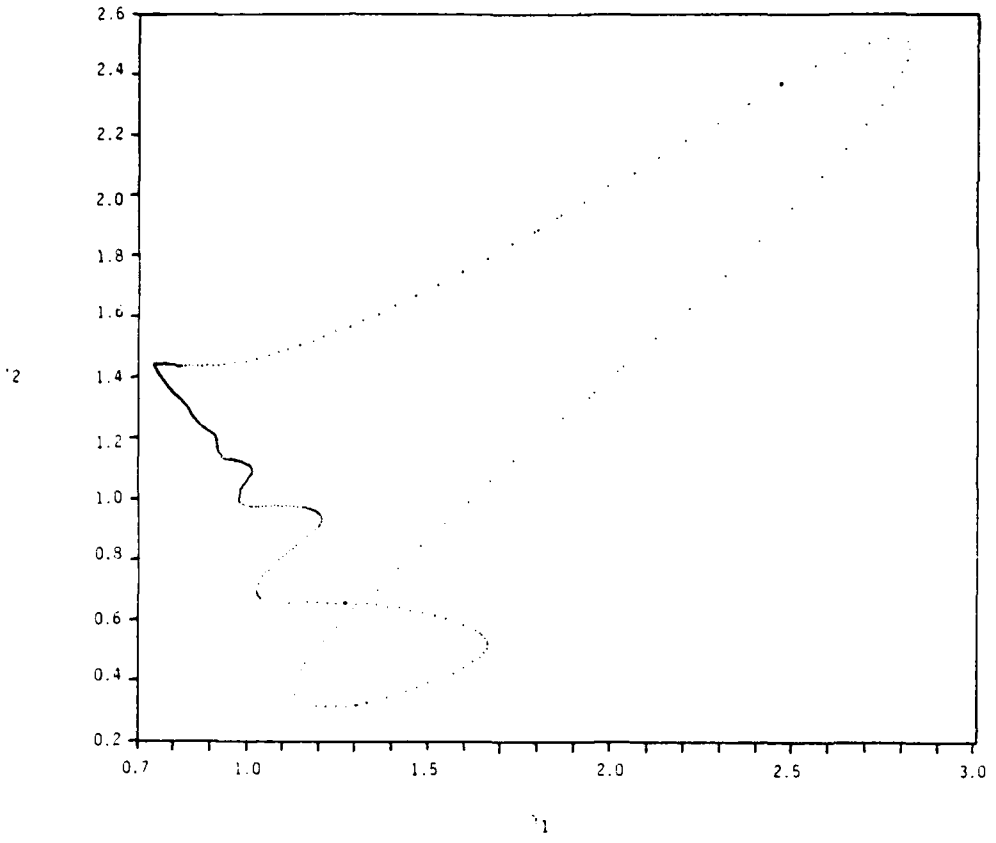

Figure 4. A limit cycle representing self-sustaining pulsations for the two mode N_{eq} = 7.02 cavity at g_oL = 7.0.

Next, the integration accuracy and the effects of including more modes into the calculation were examined. Figure 5 plots the mirror amplitude (x) for a cavity with Neq = 6.5 with the number of longitudinal integration points set at n_{slab} = 5, 15, 25, and 45. Also given in Table II are the amplitudes and phases for various integration meshes. Evidently, increasing the accuracy from n_{slab} = 15 leads to little noticeable change in the results. As expected from previous thin slab calculations where as little as one slab was used, great accuracy of integration in the longitudinal direction is not needed. For all of these calculations 512 transverse points were used. These are not spread uniformly, but are concentrated near the center of the cavity due to the exponential Gardiner transformation used in the FHT algorithm[16]. This number of points was adequate to treat the transverse field dependence of cavities with N $\sim$ 10.

It was expected that a small number of modes would be necessary to describe the nonlinear behavior, and indeed for most cases three to four modes gave essentially the same results as six modes. Table III gives the amplitudes and phases for both cavities considered at g_0L = 5 with the number of modes increased from 1 to 6. The modes are ordered according to loss, and it is evident that the more lossy modes have smaller amplitudes. For the Neq = 6.5 cavity, the lowest loss mode is by far the largest with about 94% of the energy. The γ_5 parameter for Neq = 6.5 appears to be quite large, however this represents only about 3% of the energy. For the Neq = 7.02 cavity, the first mode has 59% and the second 36% of the energy, more evenly distributed since the coupling is not quite strong enough at g_0L = 5 to suppress either of the lowest loss modes.

To demonstrate the effect of gain on the distribution of the cavity radiation, Figures 6 and 7 compare the six mode g_0L = 5 result for $|\phi|$ with the empty resonator g_0L = 0 results. The radiation in the Neq = 6.5 cavity, with 94% of the energy in the lowest loss mode, is little affected by the gain. The main difference between the curves is that the distribution in the saturable gain medium is more strongly suppressed near the mirror edge. The bumps and valleys of the curves match quite well, showing indeed that the empty resonator modes give a good description of loaded cavity behavior. On the other hand, the

Table II. Amplitudes, relative phases, and frequency shift for the six mode N_{eq} = 6.50 cavity for a range of z-integration grids.

	n_{slab} z				
	5	15	25	35	45
γ_1	1.532	1.350	1.364	1.359	1.359
γ_2	0.214	0.127	0.118	0.121	0.121
γ_3	0.105	0.130	0.141	0.142	0.141
γ_4	0.089	0.068	0.061	0.064	0.064
γ_5	0.291	0.266	0.265	0.265	0.266
γ_6	0.062	0.020	0.021	0.020	0.019
$\theta_2-\theta_1$	148.52	160.14	170.67	168.38	168.03
$\theta_3-\theta_1$	-120.39	-98.33	-105.31	-103.87	-103.77
$\theta_4-\theta_1$	150.15	131.58	132.75	131.98	131.70
$\theta_5-\theta_1$	-88.39	-86.08	-85.20	-85.26	-85.26
$\theta_5-\theta_1$	-114.47	-106.64	-109.33	-111.25	-110.50
$\Delta\omega(c/2L)$	-0.222	-0.223	-0.208	-0.209	-0.209

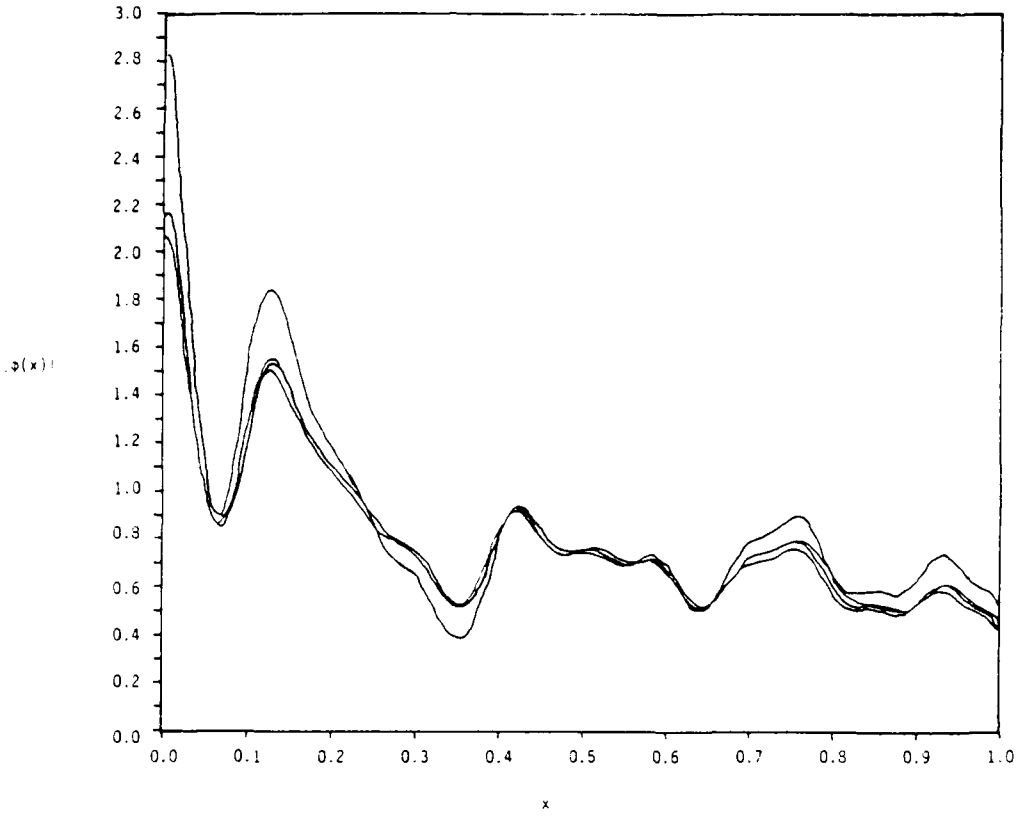

Figure 5. Plots of the mirror amplitudes $|\phi(x)|$ for the six mode $n_{eq} = 6.5$ $g_0L = 5$ cavity with 5, 15, 25, and 45 points in the z-interpolation grid. The distributions converge rapidly to the $n_{slab} = 45$ result.

Table III. Amplitudes, relative phases, and total frequency shifts for the M = 2, N_{eq} = 6.5 cavity with g_0L = 5. Up to six modes are included, and in all cases 45 longitudinal slabs were used in the z-integration.

	n=1	n=2	n=3	n=4	n=5	n=6
γ_1	1.462	1.490	1.431	1.443	1.353	1.359
γ_2	-----	.179	.165	.153	.130	.121
γ_3	-----	-----	.125	.128	.141	.141
γ_4	-----	-----	-----	.079	.064	.064
γ_5	-----	-----	-----	-----	.265	.266
γ_6	-----	-----	-----	-----	-----	.019
$\Delta\omega(c/2L)$	-.102	-.049	-.050	-.050	-.210	-.210
$\theta_2-\theta_1$	-----	174.83	163.09	163.09	167.06	168.02
$\theta_3-\theta_1$	-----	-----	-94.33	-87.28	-104.38	-103.77
$\theta_4-\theta_1$	-----	-----	-----	137.51	131.63	131.70
$\theta_5-\theta_1$	-----	-----	-----	-----	-85.26	-85.26
$\theta_6-\theta_1$	-----	-----	-----	-----	-----	-110.50

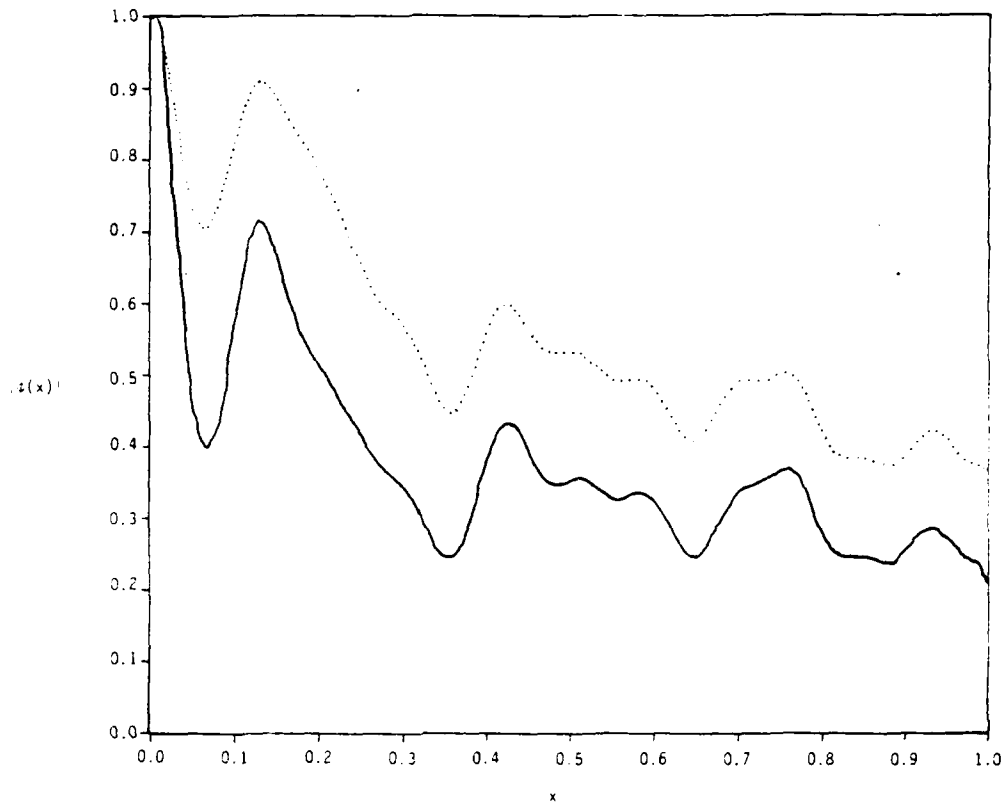

Figure 6. The six mode mirror amplitude $|\phi(x)|$ for the $N_{eq} = 6.5$ $g_o L = 5$ cavity with 45 points in the z-integration grid is compared with the lowest loss mode of the corresponding empty resonator (dotted line).

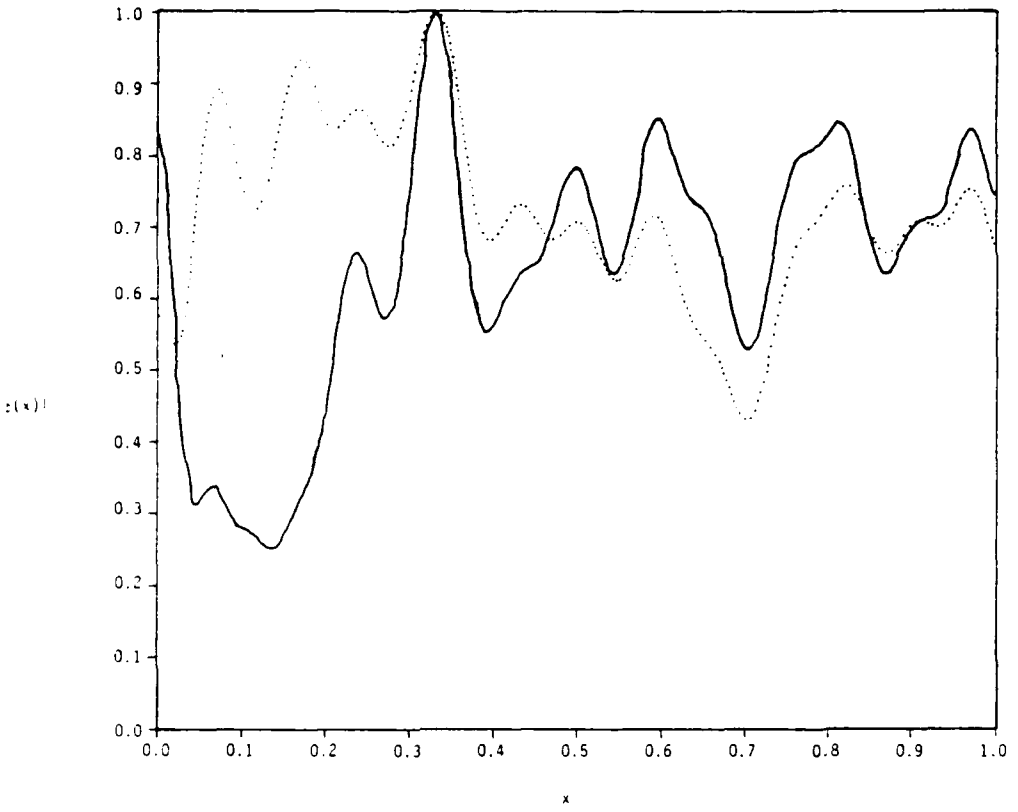

Figure 7. The six mode mirror amplitude $|\phi(x)|$ for the $N_{eq} = 7.02$ $g_o L = 5$ cavity with 45 points in the z-integration grid is compared with one of the lowest loss modes of the corresponding empty resonator (dotted line).

Neq = 7.02 solution exhibits significant deviations from the empty resonator mode as expected since the two lowest loss modes are of equal importance. Evidently the empty resonator modes best characterize loaded cavities when a single mode absorbs most of the energy.

Next, the effect of nonlinear gain on frequency pulling and output couplings was considered. These quantities are determined by cavity geometry and diffractive effects for empty resonators. The frequency shift of the Neq = 6.5 cavity with $g_0L = 5$ was $\Delta\omega = -.20\ c/2L$, and the Neq = 7.02 cavity was frequency shifted a much larger value $\Delta\omega = -.51c/2L$. In the first case the frequency pulling is much larger than the empty resonator diffractive frequency shift found in Table I. The large frequency shift for the Neq = 7.02 case, equivalent to 1/2 of the longitudinal spacing, is typical for cavities operating near a crossing of eigenvalues. It is apparent that the saturable gain medium can affect frequency pulling at least as much as diffraction.

The effective output couplings for the two cases, given by Eq. (24), were 72.8% for the Neq = 6.5 cavity, and 66.3% for the Neq = 7.02 cavity. By comparison, the geometric optics loss in both cases is 75%. Note that the Neq = 7.02 cavity has losses determined almost entirely by the two crossed modes with 64% losses. On the other hand, the Neq = 6.5 lowest loss is only 61%, while the effective loaded cavity losses are 73%. Coupling to the higher order modes greatly increases the losses in this case, and it is not understood why a similar effect does not occur for the two mode $N_{eq} = 7.02$ cavity.

To determine the fits to the Van der Pol form in the vicinity of the stable points, γ_i's were varied randomly in a region within 1% of their stable values, and the phases $_i$ were kept fixed. For each set of amplitudes chosen this way, the $\dot{\gamma}_i$ and $\dot{\theta}_i$ were calculated using the overlap integral procedure. A large number of these points enabled the α, β, σ, ρ parameters to be determined by least squares fitting.

For this procedure to give reasonable results, the amplitudes of the modes should vary less than 1% from their stable point values when noise fluctuations are allowed for. From Eq. (32) it can be seen that in order for the amplitude fluctuations to be less than 1%, D must be less than 10^4. D is determined from laser parameters by Eq. (36), and using some typical parameters

$$\begin{aligned} \gamma &= 10.6 \\ N_2 &= 6.0 \text{ Torr} \\ t_2 &= 2.2 \times 10^{-4} \text{ sec} \\ N &= 8.67 \\ I_s &= 1 \text{ watt - cm}^{-2} \\ L &= 100 \text{ cm} \end{aligned} \tag{37}$$

results in the value $D = 1.34 \times 10^{-9}$, which implies fluctuations much less than 1%.

Consider first the case of only two competing modes. The fitted parameters for the two cases at $g_0 L = 5$ are given in Table 6. The stability analysis of two mode operation involves the effective gain parameters α_1' and α_2', and the coupling constant C defined by[2]:

$$\alpha_1' = \alpha_1 - \beta_{12}\alpha_2/\beta_{22}$$

$$\alpha_2' = \alpha_2 - \beta_{21}\alpha_1/\beta_{11} \tag{38}$$

$$C = \beta_{12}\beta_{21}/\beta_{11}\beta_{22}$$

For the Neq = 6.5 cavity, the parameters in Eq. (38) are given by $C = 2.23 \times 10^{-3}$, $\alpha_1' = .307$, and $\alpha_2' = .212$. Since $C<1$, linear stability analysis implies the existence of a stable point with both modes oscillating at

γ_1 = 1.526 and γ_2 = .170. This is the stable point that is actually found. On the other hand, the N_{eq} = 7.02 cavity has C = 4.43, α_1' = -.520, and α_2' - .249. This is strong coupling, and the two possible stable solutions each have one mode totally suppressed. The actual solution found has both modes oscillating with γ_1 = .832 and γ_2 = .771. According to linear stability analysis, this solution, though stationary, is not stable with respect to small perturbations. The fact that our solution is indeed stable indicates that the fit to the Van der Pol form has limited usefulness when both modes are oscillating. For larger gains, one of the N_{eq} = 7.02 modes was indeed suppressed and the Van der Pol fits were consistent.

The Neq = 6.5 cavity with g_0L = 5 appears to be well described by the Van der Pol fit in the vicinity of the stable point. The parameters for the 1, 2, 3, and 4 mode calculations for this case are given in Table 6. With D chosen as D = 10^{-9} power fluctuations are found to be of magnitude $\Delta I/I \sim 10^{-4}$.

The linewidths are given by the F.W.H.M. values of the P(δw) curves, and may be found directly from Eq. (31). The results for both the linewidths and frequency pulling are given in Table V. Increasing the number of modes considerably changes the single mode results, even though over 90% of the energy is concentrated in the lowest loss mode. The frequency broadening effects do not change much as the number of modes becomes greater than 1, indicating that a description with just a few modes gives reasonably consistent results. Note that The frequency broadening effects considered here arise from amplitude fluctuations and mode couplings, not phase fluctuations.

Table IV. The fitted Van der Pol parameters α_i, γ_i, β_{ij}, and ρ_{ij} for the N_{eq} = 6.50 cavity with one to four modes.

	α	σ	β				ρ			
n=1	0.736	-0.147	0.330				-0.034			
n=2	0.612	-0.565	0.265	-0.093			-0.239	0.419		
	0.209	-0.008	-0.093	14.656			0.419	-32.584		
	0.714	-0.372	0.349	-0.794	-0.618		-0.166	0.989	-0.880	
n=3	-1.000	1.174	-0.794	22.009	10.157		0.989	-41.196	-0.125	
	-0.761	-1.027	-0.618	10.157	16.292		-0.880	-0.125	42.865	
	1.670	-0.913	0.804	-1.117	-1.958	-1.499	-0.436	0.907	-0.717	10.630
n=4	-1.853	1.094	-1.117	20.603	8.596	-6.887	0.907	-40.105	-1.264	2.578
	-3.644	-0.719	-1.958	8.596	19.695	12.420	-0.717	-1.264	48.643	-1.299
	-3.119	20.599	-1.499	-6.887	12.420	8.924	10.630	2.578	-1.299	-640.876

Table V. Frequency pulling and frequency broadening, in units of c/2L, for the N_{eq} = 6.50 cavity. The shift is determined by the stable solution, and the broadening by the time dependent behavior in the vicinity of the stable point under the influence of a random noise term.

	Pulling $\Delta\omega(c/2L)$	Broadening $\Delta\omega(c/2L)$
n = 1	-.072	4.39×10^{-6}
n = 2	-.022	33.24×10^{-6}
n = 3	-.023	20.32×10^{-6}
n = 4	-.018	21.45×10^{-6}

VI. CONCLUSIONS

The use of series expansions in empty resonator modes to describe lasers with nonlinear gain media has been examined. The method hinges on the evaluation of the overlap integrals, which involve double integrals over longitudinal and transverse dimensions. It has been found that ten or twenty grid points give reasonable results for the longitudinal integration, while a much larger number of points are needed for the transverse integrations. This is in accordance with thin slab approximations, which have been shown to give good results for a relatively small number of slabs.

Even though the overlap integrals are difficult, this method is still faster than direct solution of the nonlinear integral equation. Assuming that the empty resonator modes are known in advance, the overlap integrals for one iteration involve $n_{modes} \times N_{transverse} \times N_{slab}$ complex additions. By contrast, one iteration of the nonlinear integral equation involves $3 \times N_{slab}$ fast hankel transforms, or $6 \times N_{slab} \times N_{transverse} \times \log_2(4N_{transverse})$ complex multiplications, and an equivalent number of complex additions. Since multiplications are about ten times more time consuming than additions and $n_{modes} \sim 3$, it is evident that the series expansion approach using overlap integrals can be much more numerically efficient than direct solution of the nonlinear integral equation. Provided the series approach also gives results equivalent to the more exact integral equation method, a significant increase in efficiency may be achieved together with more direct physical interpretation of the solutions.

The results appear to be best for cavities operating far from the crossing points of the eigenvalue plot. In this regime, the lowest loss mode is well separated and the series expansion gives reasonable results with the largest part of the energy is concentrated in only one mode. A three or four mode description was sufficient to characterize the response of the resonator to a nonlinear gain medium, and the radiation pattern was qualitatively and quantitatively quite similar to that of the empty resonator mode. By contrast, the effective output coupling, frequency pulling, and linewidth varied

considerably from the empty resonator results. The nonlinear effects of the additional lossy modes are to increase the output coupling and to both broaden and shift the laser frequency.

In general, the solution to an equation with a nonlinear source term cannot be expressed as a linear superposition of solutions to the homogeneous equation. Only when one of the resulting expansion coefficients is much larger than the others should the series expansion be considered as a numerically accurate solution to the nonlinear problem. If one is interested mostly in quantitative results, the method of using series expansions in empty resonator modes should be used only if one mode dominates.

However, the series expansion approach can always be used to characterize the qualitatiave behavior of high energy systems. In particular, this approach is the lowest level of approximation at which pulsations, bistability, and chaotic behavior involving competition between transverse modes can be expected to occur. The geometric optics approximation cannot lead to this type of unstable behavior, and the nonlinear integral equation is not applicable in the region of chaos or pulsations. Consequently, the equations of motion of the laser using series expansions in empty resonator modes may be the best available way to characterize such systems.

We have not considered here pulsed mode operation, or frequency dependent gain. Pulsed operation may be treated by allowing the expansion coefficients to have a slowly varying z dependence, which adds a z derivative to the equations of motion[9]. More complicated time dependence may be treated by directly solving the equations of motion rather than simply determining the stable points. Frequency dependent gain complicates the problem because the equations are no longer first order in time derivatives. These difficulties have been resolved for lasers with stable cavities[27] and therefore the same methods should be applicable for unstable resonator cavities.

REFERENCES

1. W.E. Lamb, "Theory of an optical maser," P.R. 134A, 1429 (1964).

2. M. Sargent, M.O. Scully, and W.E. Lamb, Laser Physics (Addison Wesley, Reading, Mass., 1974).

3. H. Kogelnik and T.Li, "Laser Beams and Resonators," Proc. IEEE 54, 1312-1329 (1966).

4. A.E. Siegman, "Unstable Optical Resonators," Appl. Opt. 13, 353-367 (1974).

5. A.G. Fox and T.Li, "Resonant Modes in a Maser Interferometer," Bell Syst. Tech. J. 40, 453-488 (1961).

6. P. Horwitz, "Asymptotic Theory of Unstable Resonator Modes," JOSA 63, 1528-1543 (1973).

7. R.R. Butts and P.V. Avizonis, "Asymptotic Analysis of Unstable Laser Resonators with Circular Mirrors," JOSA 68, 1072-1078 (1978).

8. J. Nagel and D. Rogovin, "Analytic Variational Method for Determining the Modes of Marginally Stable Resonators," JOSA 70, 1525-1538 (1980).

9. A.E. Siegman, "Exact Cavity Equations for Lasers with Large Output Coupling," Appl. Phys. Lett. 36, 412-414 (1980).

10. D. Newman and S. Morgan," Existence of Eigenvalues for the Integral Equations in Laser Theory," Bell Syst. Tech. J. 43, 113,126 (1964).

11. J. Cochran, "The Existence of Eigenvalues for the Integral Equations in Laser Theory," Bell Syst. Tech. 44, 77-88 (1965).

12. H. Hochstadt, "Integral Equations in Laser Theory," SAIM Review 8, 62-65 (1966).

13. I.F. Balashov and U.A. Berenberg," Nonstationary Modes of an Open Resonator," Sov. J. Quant. El. 5, 159-161 (1975).

14. A.E. Siegman, "Orthogonality Properties of Optical Resonator Eigenmodes," Opt. Comm. 31, 369-373 (1979).

15. H. Statz and C.L. Tang," Problem of Mode Deformation in Optical Masers," J. Appl. Phys. 36, 1816-1819 (1965).

16. A. Fox and T. Li, "Effect of Gain Saturation on the Oscillating Modes of Optical Masers," IEEE J. Quant. El. QI-2, 774-793 (1966).

17. D.B. Rensch and A.N. Chester, "Iterative Diffraction Calculations of Transverse Mode Distributions in Confocal Unstable Laser Resonators," Appl. Opt. 12, 997,1010 (1973).

18. Y. Karamzin and Y. Konev, "Numerical Investigation of the Operation of Unstable Telecopic Resonators Allowing for Diffraction and Saturation in the Active Medium," Sov. j. Quant. El. 5, 144-148 (1975).

19 W.H. Louisell, in Physics of Quantum Electronics, edited by S.F. Jacobs, M.O. Scully, M. Sargent, and C.D. Cantrell (Addison-Wesley, Reading, Mass., 1976), Vol. 3, P. 369.

20. G.P. Agrawal and M. Lox, Effects of Interference on Gain Saturation in Laser Resonators," JOSA 69, 1717-1719 (1975).

21. A.E. Siegman, "A Quasi-Fast Hankel Transform," Opt. Lett. 1, 3 (1977).

22. H.M. Gibbs, F.A. Hopf, D.L. Kaplan, and R.L. Shoemaker, "Observation of Chaos in Optical Bistability," Phys. Rev. Lett. 46, 474-476 (1981).

23. H. Haken, Synergetics (Springer-Verlag, Berlin, 1977).

24. A. Yariv, Quantum Electronics (Wiley, New York, 1975).

25. W.W. Rigrod, "Saturation Effects in High Gain Lasers, "J. Appl. Phys. 36, 2487-2490 (1965).

26. T. Bischofberger and Y.R. Shen, "Theoretical and Experimental Study of the Dynamic Behavior of a Nonlinear Fabry-Perot Interferometer," Phys. Rev. 19A, 1169-1176 (1979).

27. L.W. Casperson, "Stability Criteria for Non-Doppler Lasers," Phys. Rev. 23A, 248-260 (1981).


DA
FILM